

Diagnostic and prognostic model studies of the Adriatic Sea general circulation: Seasonal variability

M. Zavatarelli, N. Pinardi, V. H. Kourafalou,¹ and A. Maggiore²

Laboratorio di Simulazioni Numeriche del Clima e degli Ecosistemi Marini, Università degli Studi di Bologna, Ravenna, Italy

Received 3 January 2000; revised 7 August 2001; accepted 23 August 2001; published 5 January 2002.

[1] The climatological seasonal variability of the Adriatic Sea general circulation is studied by carrying out diagnostic and prognostic numerical experiments. Two different sets of European Centre for Medium-Range Weather Forecasts-derived forcing functions were used to drive the model, because of the uncertainties in the heat and momentum flux determination, and the results are compared. The diagnostic simulations allowed a comparison of the model solutions with the observed baroclinic general circulation, and the results, in agreement with recent observations, suggest that during winter the Western Adriatic Coastal Current has a significant barotropic component, while during summer all the general circulation features are largely baroclinic. The prognostic simulations indicated that the circulation has a large seasonal variability, whose amplitude may be affected by the strength of the wind-forcing field. *INDEX TERMS:* 4219 Oceanography: General: Continental shelf processes, 4243 Oceanography: General: Marginal and semiencllosed seas, 4255 Oceanography: General: Numerical modeling; *KEYWORDS:* Adriatic Sea, Mediterranean Sea, seasonal circulation, continental shelf processes, marginal and semiencllosed seas, numerical modeling

1. Introduction

[2] Despite being one of the most studied regional seas of the world the Adriatic Sea (Figure 1) still lacks Comprehensive numerical modeling studies aimed at the definition of the variability of the seasonal circulation at the climatological scale. The reason for that probably lies in the complexity of its general circulation processes determined by the atmospheric forcing, basin morphology, river runoff, and outflow/inflow system at the Otranto Channel.

[3] Shaped as an elongated basin with its major axis in the NW-SE direction, communicating with the Ionian Sea through the Otranto Channel to the south, the Adriatic Sea is almost entirely surrounded by mountain ridges: the Apennine to the west, the Alps to the north, and the Dinaric Alps to the east. These determine a strong topographic control of the wind field, particularly in the northern part of the basin, where strong, episodic NE winds (the so-called “Bora” or “Bura”) channeled by the opening between the Alps and the Dinaric Alps occur during winter. The other main wind affecting the basin general circulation, mainly in spring and autumn, is a SE wind (the so-called “Scirocco” or “Sirocco”), also influenced by the orography, being channeled along the major axis of the basin by the Apennine and the Dinaric Alps [Cavaleri *et al.*, 1996].

[4] The bottom morphology (Figure 1) identifies three major subbasins: the northern, the middle, and the southern. The northern Adriatic part is very shallow (average depth: 35 m), the middle Adriatic (average depth: about 140 m) is characterized by two bottom depressions (the so-called “Pomo” or “Jabuka” Pits), reaching about 250 m depth. The southern Adriatic is characterized by a strong topographic gradient, leading to a wide depression

having a maximum depth of about 1200 m. Therefore the north to south topographic gradient determines the close coexistence of a northern subbasin, characterized by truly shelf and coastal conditions, with a southern subbasin having open ocean characteristics. A very important component of the forcing functions of the circulation is given by the large number of freshwater sources distributed along the portions of the Adriatic coast indicated in Figure 1.

[5] The seasonal climatology of the forcing functions (wind stress, heat fluxes, and freshwater fluxes) has been recently analyzed by Raicich [1994a, 1994b; 1996]; Artegiani *et al.* [1997a] and Maggiore *et al.* [1998] on the basis of existing available data sets. The basin-averaged heat flux is negative and amounts to about -22 W m^{-2} [Artegiani *et al.*, 1997a]. The largest heat losses occur in winter (about 250 W m^{-2}), while the largest heat gains occur in summer (about 200 W m^{-2}). A net heat input at the Otranto Channel should compensate the net surface heat loss. Conversely, the water budget is positive, with an average annual water gain $>1 \text{ m}$, mostly determined by the strong river runoff contribution, since evaporation and precipitation almost cancel each other on an annual basis. The major river in the basin is the Po (see Figure 1), but other significant rivers are discharging along the whole Adriatic coast. Maximum freshwater gains occur in spring, because of both precipitation and river runoff; during summer, freshwater losses prevail in the offshore areas, while over the shelf the river runoff contribution remains dominant. Therefore the heat and freshwater fluxes have an overall opposite effect on the buoyancy forcing, with the possibility of density compensation processes affecting the overall thermohaline circulation and probably also local circulation features [Hopkins *et al.*, 1999]. This will be discussed mainly in part 2 of this paper (M. Zavatarelli *et al.*, manuscript in preparation, 2002). The process of dense water formation occurs at two distinct locations: the shallow northern Adriatic [Artegiani *et al.*, 1989] and the deeper southern Adriatic [Ovchinnikov *et al.*, 1987] with different characteristics.

[6] Artegiani *et al.* [1997a, 1997b] (hereinafter referred to as A97a and A97b) produced a detailed analysis of the Adriatic

¹Now at National Center for Marine Research, Athens, Greece.

²Now at Royal School of Mines, Imperial College, London, UK.

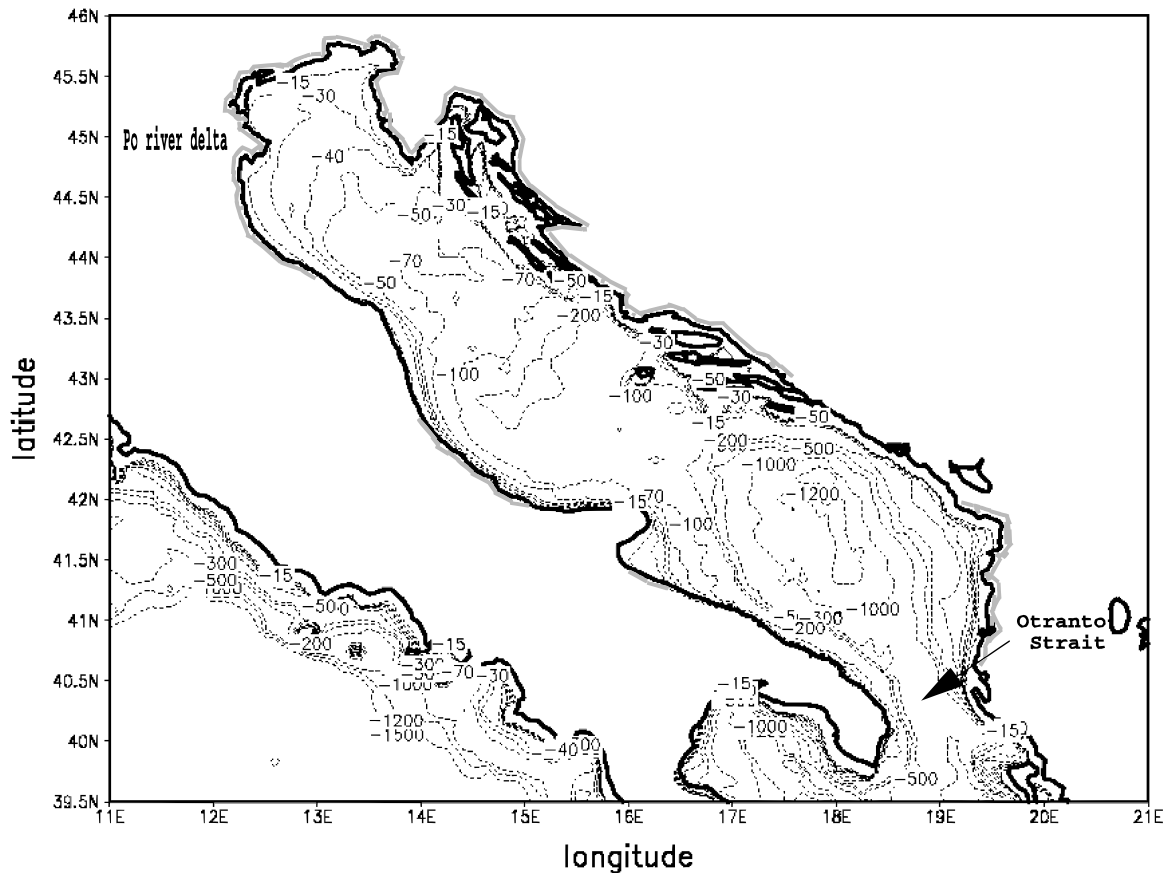


Figure 1. The Adriatic Sea coastal morphology. The shaded areas along the coastline indicate the regions of freshwater inputs into the basin.

Sea general circulation, at the seasonal climatological level, based on historical hydrological data. Their analysis defined the three main Adriatic water masses (surface, intermediate, and deep) present in the three major subbasins. The local hydrological characteristics depend, at the surface, on the degree of dilution induced by the freshwater input; at intermediate level, on the extent of the Levantine Intermediate Water penetration into the basin; and at depth, on the dense water formation and spreading processes. Moreover, they calculated dynamic height climatological maps, thus inferring the seasonal characteristics of the Adriatic Sea large-scale baroclinic general circulation. Coastal currents, jets, and cyclonic gyres, whose strength varies seasonally, compose the resulting geostrophic circulation. A97b named the most important circulation features: the three segments (northern, middle, and southern) of the current flowing southward along the western coast of the Adriatic Sea, here defined as Western Adriatic Coastal Current (WACC), and the Eastern Southern Adriatic Current (ESAdC), flowing northward along the eastern coast of the southern Adriatic. These currents interact with three major cyclonic gyres located in the northern (NAd), central (MAd), and southern (SAd) subbasins.

[7] Poulain [2001] (hereinafter referred to as P01) devised a description of the Adriatic Sea surface seasonal circulation based on the results of extensive Lagrangian experiments carried out in the basin during the past decade. The descriptions of the surface circulation proposed by A97b and P01 are not consistently comparable because one treats the baroclinic component of the general circulation only and the other treats

the complete velocity field; however, they show several points of agreement, namely, the basinwide cyclonic pattern, the pronounced offshore extension of the WACC in summer in contrast with the winter season.

[8] From a numerical modeling point of view, previous studies focused mainly on the barotropic circulation or on the definition of process studies with a particular emphasis on the effect of transient Bora wind episodes and the Po River thermohaline forcing on the northern Adriatic Sea circulation. *Malanotte Rizzoli and Bergamasco* [1983] carried out the first modeling attempt with a multilevel model implemented in the northern Adriatic area. They found that the Northern Adriatic circulation in winter was strongly connected to thermohaline forcing as well as to wind forcing. More recently, *Orlic et al.* [1994], with a barotropic model, and *Bergamasco and Gacic* [1996] investigated the response of the whole Adriatic basin to the dominant Bora and Scirocco winds. *Kuzmic* [1991], *Schrimpf et al.* [1992], and *Bone* [1993] carried out regional process studies, mostly focusing on the effect of Bora on the northern Adriatic barotropic circulation. A process study aimed to simulate the dense water formation process in the northern Adriatic Sea was performed by *Vested et al.* [1998] utilizing a nonhydrostatic model. Numerical process studies were also carried out to study the development and the evolution of the Po river plume under variable conditions of buoyancy and wind stress forcing [*Kourafalou*, 1999]. All these studies identified the importance of the wind and thermohaline forcing on the circulation structure but failed to compare with a comprehensive set of observations because of the idealized

nature of the modeling exercise or the absence of reliable climatological information.

[9] Here we show and discuss the results of a diagnostic and prognostic numerical model study on the general circulation of the Adriatic sea, carried out utilizing a fully three-dimensional numerical model forced with a complete set of climatological forcing functions. In this first part we focus on the definition and description of the seasonal variability of the circulation. Emphasis is put on the wind and the thermohaline forcing, aiming to complement the information arising from the data analysis of A97b and the previous modeling studies. One of the novelties of the paper is the comparison between diagnostic and prognostic simulations, which will allow the partial validation of the modeling results. In addition, the realistic simulation of the circulation seasonal cycle is shown for the first time. In M. Zavatarelli et al. (manuscript in preparation, 2002) the role of buoyancy versus wind forcing on the circulation will be explored, and the estuarine/antiestuarine circulation components will be elucidated.

[10] Section 2 describes the characteristics of the model used, along with details of the Adriatic Sea implementation, the forcing functions, and the numerical experiments carried out. Section 3 describes the seasonal variability of the circulation resulting from the diagnostic experiments. Section 4 shows the prognostic calculations, and section 5 offers conclusions.

2. Model Design

2.1. General

[11] The ocean model used is the Princeton Ocean Model (POM) [Blumberg and Mellor, 1987]. It is a three-dimensional, finite difference, free-surface numerical model utilizing the Boussinesq and the hydrostatic approximation and a split mode time step. The model contains a second-order turbulence closure submodel providing the vertical mixing coefficients [Mellor and Yamada, 1982]. Horizontal diffusion coefficients are calculated with a Smagorinsky [1993] formulation, implemented into POM according to Mellor and Blumberg [1986]. Density is calculated by an adaptation of the UNESCO equation of state devised by Mellor [1991]. A description of the model code is given by Mellor [1998]. A listing of the model free parameters adopted in the present study is given in Table 1.

2.2. Model Grid and Bathymetry

[12] We used the curvilinear grid shown in Figure 2. It encompasses the whole Adriatic basin and extends south of the Otranto Channel into the northern Ionian Sea where the only open boundary is located. It has a variable resolution ranging from 3–5 km in the northern Adriatic to 10–12 km in the southern part of the model domain.

[13] In the vertical, POM uses a bottom-following sigma coordinate system $\sigma = (z - \eta)/(H + \eta)$, where $H(x, y)$ is the bottom topography and $\eta(x, y)$ is the free-surface elevation. In the present

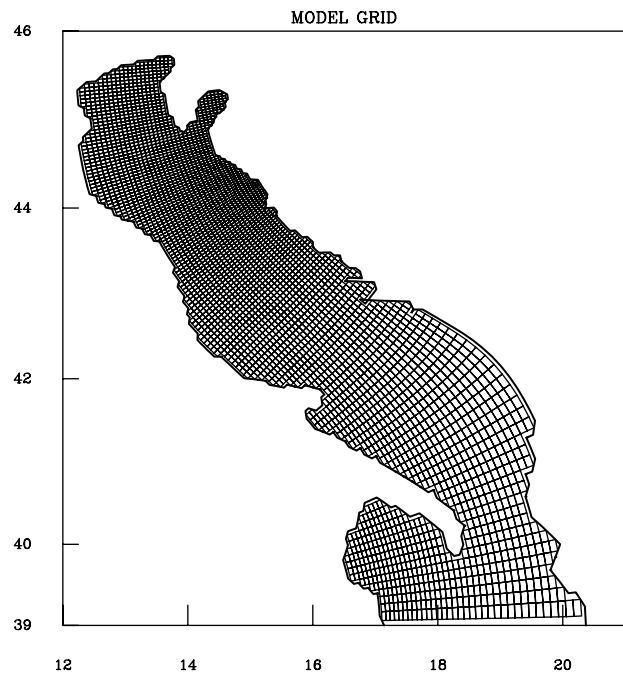


Figure 2. The model curvilinear orthogonal grid.

study the model has 21 vertical sigma levels, more compressed near the surface and the bottom.

[14] The model bathymetry was obtained from the U.S. Navy 1/12° Digital Bathymetric Data Base 5 (DBDB5) by bilinear interpolation of the depth data in the model grid. The original DBDB5 depth data relative to the northern Adriatic Sea were found to be incorrect, and it has been necessary to correct the database by inserting depth data obtained by a nautical map. Some simplification of the coastline was carried out along the eastern coast where the Dalmatian islands were either eliminated or joined to the mainland because of the poor definition of the coastline in the database (see Figures 1 and 2). The minimum depth was set to be 20 m. The external and internal mode time steps were chosen to be 20 and 1000 s, respectively.

2.3. Initial Conditions

[15] Temperature and salinity for the diagnostic and prognostic experiments were obtained from the A97a and A97b data set updated with stations having bottom depth shallower than 15 m. However, since this data set (originally named Adriatic Temperature, Oxygen and Salinity data set (ATOS)) has no data south of the Otranto Channel, in order to cover the Ionian sector of the model domain and to prepare the initial condition fields to the specification of the open boundary conditions values (see below) a new data set was constructed (named ATOSMOM) by merging the A97a and A97b data with monthly values of temperature and salinity data (pertinent to the Ionian Sea only) obtained from the perpetual year forcing 0.25° resolution Mediterranean Sea implementation of the Modular Ocean Model (MOM) [Roussenov et al., 1995; Castellari, 1996]. The model data were merged with the A97a, A97b data inside the Adriatic using objective analysis techniques as by A97b.

[16] A97a defined four seasons on the basis of the analysis of the Adriatic Sea heat storage annual cycle. They are winter, January to April; spring, May to June; summer, July to October; and autumn, November to December. This definition has been adopted to calculate the seasonal averages.

Table 1. Model Free Parameters

	Description	Value
C	nondimensional constant used in calculating the horizontal viscosity	0.1
μ_M	background diffusivity	$10^{-5} \text{ m}^2 \text{ s}^{-1}$
Z_0	bottom roughness length	0.01 m
λ	solar radiation attenuation coefficient	0.042 m^{-1}
Tr	nondimensional transmission coefficient for solar radiation penetration	0.31

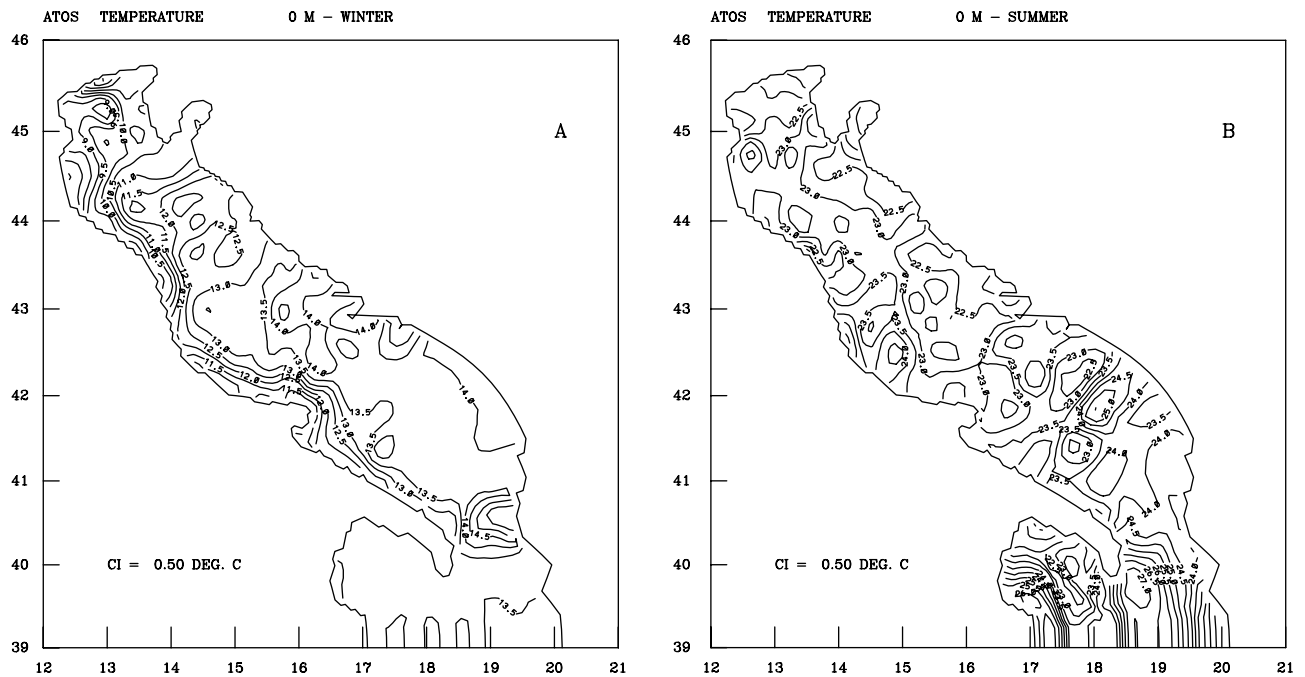


Figure 3. Seasonal surface temperature distribution from the ATOSMOM database interpolated in the model curvilinear grid: (a) winter and (b) summer. The contour interval is 0.5°C .

[17] The seasonal surface temperature and salinity fields obtained are shown in Figures 3 and 4, respectively. These analyses are similar to those produced by A97b, but they needed to be redone for the model grid and are shown for consistency. To be noticed are (1) the large temperature gradient in winter between the Italian shelf areas and the rest of the basin; (2) the smaller-scale spatial variability of the temperature field in summer, indicative either of unresolved mesoscale features in the climatology or realistic smaller scale

spatial variability; and (3) the large salinity gradient in the western coastal areas, evidencing the constant presence of the runoff signature of the northern and western Adriatic rivers. The river runoff effects on the eastern coastline are evident for the Albanian rivers, particularly in spring (not shown). Other features appearing in the maps may be due to the absence of accurate temperature and salinity data in the vicinity of the Croatian coast. Widening of the salinity front is evident in summer. The diagnostic experiments were executed utilizing

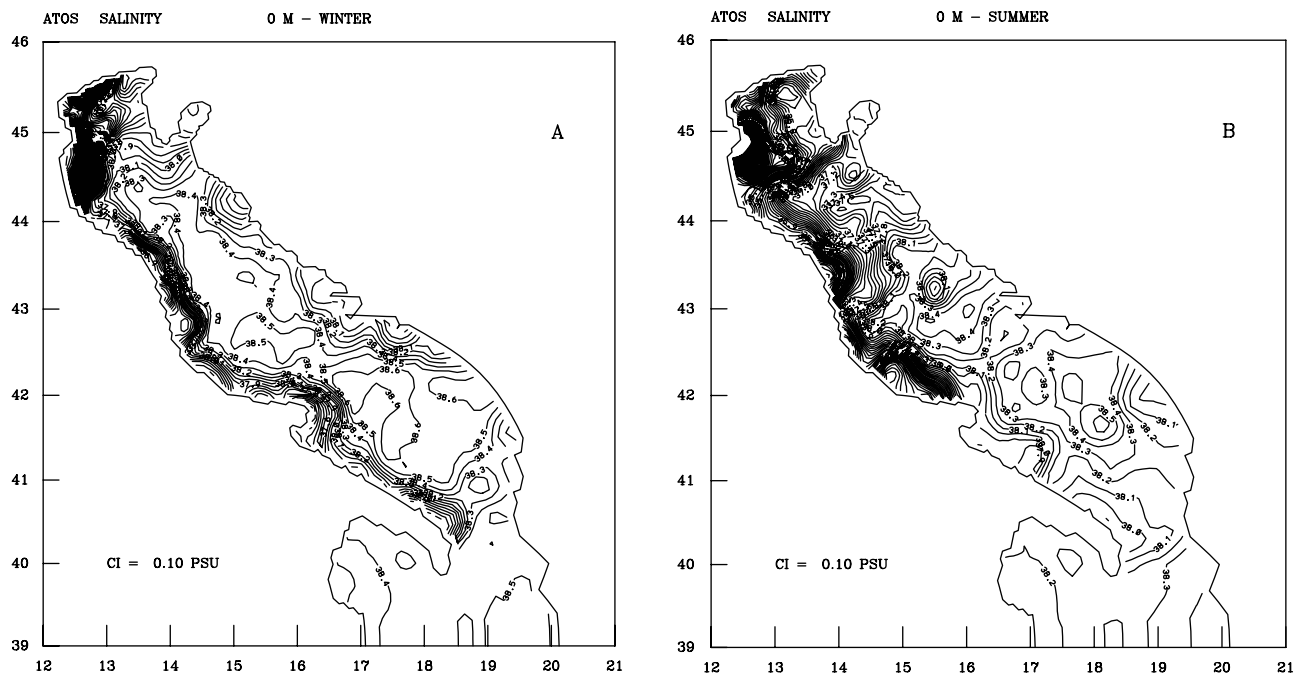


Figure 4. As in Figure 3 but for salinity. The contour interval is 0.1 psu .

Table 2. Main Characteristics of the ECMWF Data Set Used for the Heat Fluxes and Wind Stress Computation^a

Data Set	Resolution	Frequency, hours	Wind Velocity	Air Temperature	Relative Humidity	Clouds	Years
Analysis	0.5625°	6	1000 hPa	1000 hPa	1000 hPa	%	1991–1994
Reanalysis	1.1250°	6	10 m	2 m	2 m	%	1982–1993

^a Analysis, ECMWF 1000 hPa analysis; and reanalysis, ECMWF surface reanalysis corrected by the 1.5 factor as proposed by *Cavaleri and Bertotti* [1997].

these four seasonal fields, while the prognostic experiments utilized the winter fields as the initial condition.

2.4. Surface and Bottom Boundary Conditions

[18] The surface boundary conditions are surface heat, water, and momentum (wind stress) fluxes. The monthly climatological surface heat flux and wind stress boundary conditions used in the experiments were obtained utilizing the atmospheric data of two European Centre for Medium-Range Weather Forecasts (ECMWF) data sets: the 6 hour, 1000 hPa analysis fields (a description of this data set can be found at www.ecmwf.int/services/data/toga.html) and the 6 hour, surface reanalysis fields [*Gibson et al.*, 1997]. We used these two data sets because they are the best available for resolution (analysis) and time consistency (reanalysis). The ECMWF analysis data set is coming from a vertical level of the atmospheric model that is located at 1000 hPa. This choice has been made in the past to drive several ocean models [*Rosati and Miyakoda*, 1988; *Roussenov et al.*, 1995]. However, for basins of such limited extent it is possible that 1000 hPa is located too high above the sea level to provide an accurate representation of the surface parameters. Thus it was decided to use also extrapolated surface atmospheric parameters such as the reanalysis data. The surface values are obtained diagnostically using boundary layer parameterizations that consider land and sea surfaces. An example of such parameterization is given by *Miyakoda and Sirutis* [1977].

[19] The atmospheric data used to compute surface fluxes and the main characteristics of the data sets are summarized in Table 2. The sea surface temperature (SST) data needed for the surface flux computation were obtained from the *Reynolds* [1988] weekly data set. Experiments with the *May* [1982, 1986] climatologies were also carried out, but they provided unsatisfactory results.

[20] From each 6 hour field, wind stress and heat fluxes were computed on the original analysis and reanalysis grid. Therefore we used the original land-sea mask, and at each “wet” grid point we specified a SST derived from the interpolation of the *Reynolds* [1988] weekly SST data set on the grid. The computed fluxes were subsequently averaged to obtain the monthly climatological values, which were interpolated into the model curvilinear grid.

[21] The wind stress is computed using the *Hellerman and Rosenstein* [1983] formula, previously utilized in the Mediterranean Sea by *Roussenov et al.* [1995]:

$$\tau = C_D |\mathbf{v}| \mathbf{v} \quad (1)$$

where \mathbf{v} is the wind field and $C_D(T_A, T_S, \mathbf{v})$ has a complicated parametric dependence from air and SST and wind amplitude. Preliminary computation of the wind stress from the ECMWF reanalysis data indicated that the wind data were too weak, probably because of the low resolution of orography in the region. The weakness of the surface ECMWF data (at least in the Adriatic region) was described and discussed for a wave-modeling study by *Cavaleri and Bertotti* [1997]. They found that the weak winds over the Adriatic basin were mainly due to the poor resolution of the continental topographic features, in particular, the mountain ridges surrounding the basin. Moreover, they found that their wave model was correctly matching observed significant wave height data only

if both components of the wind velocity data were multiplied by a factor of 1.5. We adopted this multiplicative factor also in our wind stress computation. Conversely, wind stress computed from the ECMWF analyses gave much higher values since they were computed with the 1000 hPa winds and the correction factor was not used. The wind stress monthly averages were computed through scalar averaging.

[22] In Figure 5 are shown the seasonal climatologies of the wind stress obtained from the ECMWF reanalysis. They show signature of the Bora wind from northeast affecting almost the whole basin during winter, a general decrease of the wind stress during the spring and summer seasons, and the influence of the southeasterly Scirocco wind on the southern basin during autumn. Obviously, the monthly and seasonal average procedure smooths out strong wind (Bora and Scirocco) events, but the study of the effects of such events on the Adriatic Sea circulation is beyond the scope of this research. For a more detailed simulation of the role played by synoptic wind events the reader should refer to the model process study of *Kourafalou* [1999] carried out with the same implementation of the POM described here and utilizing synoptic wind stress fields. The climatologies obtained from the ECMWF analysis (not shown) indicate, with respect to the reanalysis seasonal fields, a larger amplitude and a stronger signature of the Scirocco in almost all seasons. Naturally, most of these differences are due to the height at which the different wind data sets are computed. The average height of the 1000 hPa is about 100 m, and we expect orographic effects to be different at this height. The basin-averaged wind stress amplitude seasonal cycle, as computed from the ECMWF reanalysis data, is shown in Figure 6, and we see that the annual mean is about 0.25 dyne cm⁻² with large seasonal excursions and minima at the end of spring and the end of summer.

[23] Heat fluxes were computed by adopting the bulk formulae described by *Castellari et al.* [1998] for the Mediterranean Sea. The computation of the total heat fluxes Q at the air sea interface is given by

$$Q = Q_s - Q_b - Q_h - Q_e. \quad (2)$$

The solar radiation Q_s has been computed according to the *Reed* [1975] formula:

$$Q_s = Q_{\text{TOT}}(1 - 0.62C + 0.019\beta)(1 - \alpha), \quad (3)$$

where Q_{TOT} is the clear-sky radiation as written by *Rosati and Miyakoda* [1988] for the world ocean, C is the fractional cloud cover, β is the noon Sun altitude, and α is the sea surface albedo computed according to *Payne* [1972]. The parameterization of *Reed* [1977] has been adopted, which considers $Q_s = Q_{\text{TOT}}$ for $C < 0.3$.

[24] The longwave radiation flux Q_b was computed using the *May* [1986] formula:

$$Q_b = [\sigma T_A^4 (0.4 - 0.05\sqrt{e_A} + 4\sigma T_A^3)(T_S - T_A)](1 - 0.75 C^{3.4}), \quad (4)$$

where σ is the Stefan Boltzmann constant, e_A is the atmospheric vapor pressure, T_S is the SST, and T_A is the air temperature.

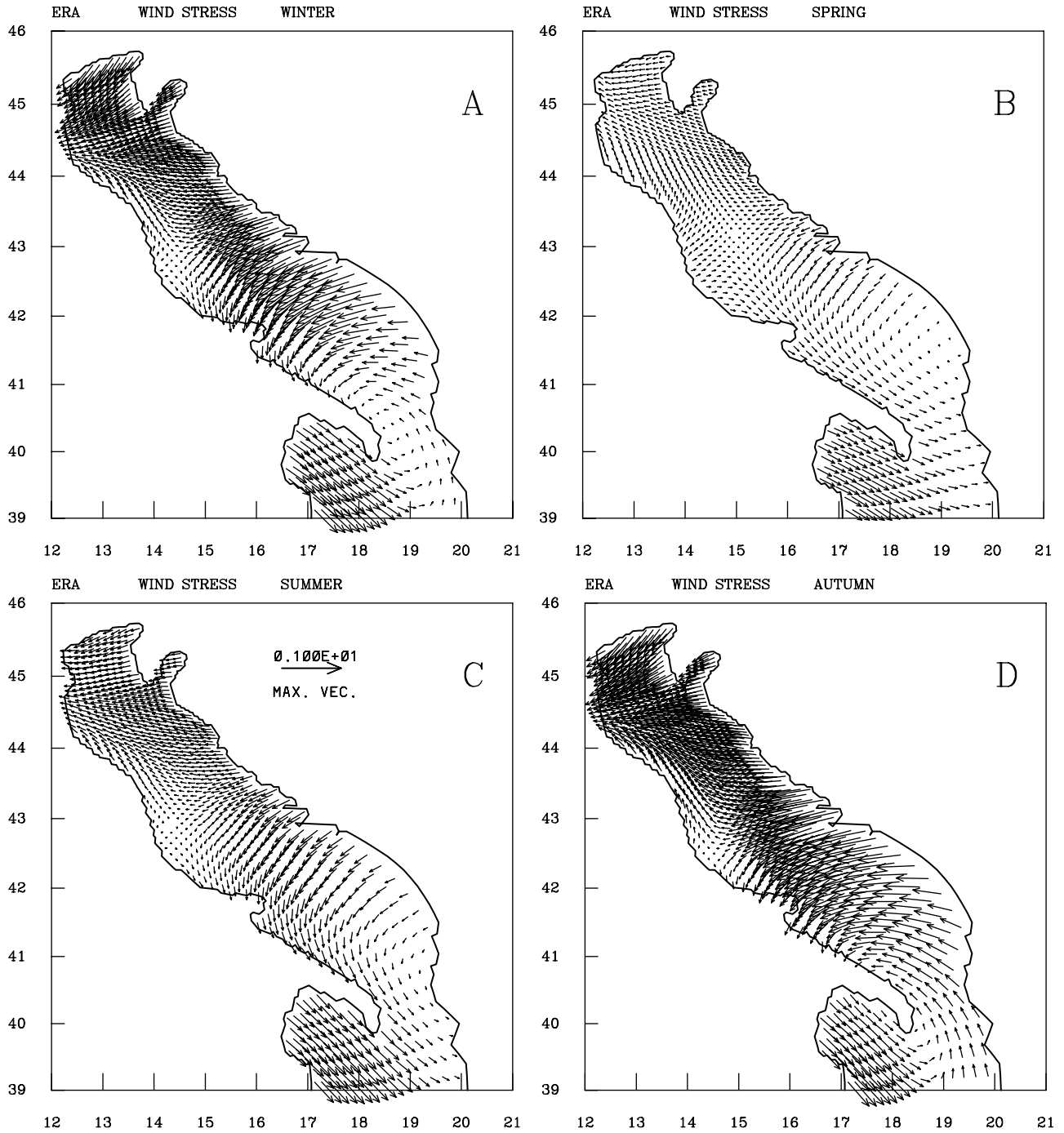


Figure 5. Seasonal climatological wind stress distribution from the ERA reanalysis: (a) winter, (b) spring, (c) summer, and (d) autumn. Units are dyne cm^{-2} .

[25] The sensible (Q_h) and latent (Q_e) heat fluxes were computed according to the classical formulas:

$$Q_h = \rho_A C_p C_H |\mathbf{v}| (T_S - T_A) \quad (5)$$

$$Q_e = L_e \rho_A C_E |\mathbf{v}| [e_{\text{sat}}(T_S) - r e_{\text{sat}}(T_A)] (0.622/p_A), \quad (6)$$

where $\rho_A = \rho_A(p, T_A, r)$ is the moist air density, C_p is the specific heat capacity at constant pressure, C_H and C_E are the turbulent

exchange coefficients computed according to *Kondo* [1975], L_E is the latent heat of vaporization, e_{sat} is the saturation water vapor pressure, r is the relative humidity, p_A is the atmospheric pressure (fixed at 1013 hPa), and $|\mathbf{v}|$ is the wind speed modulus.

[26] The estimated annual heat budget is -17 W m^{-2} for the ERA reanalysis and -19 W m^{-2} for the ERA reanalysis. In Figure 7 we show the basin average of Q and its components as computed from the ERA reanalysis. The maximum heat gain occurs from May to August, while the large heat losses (comparable to other northern Mediterranean deep water forma-

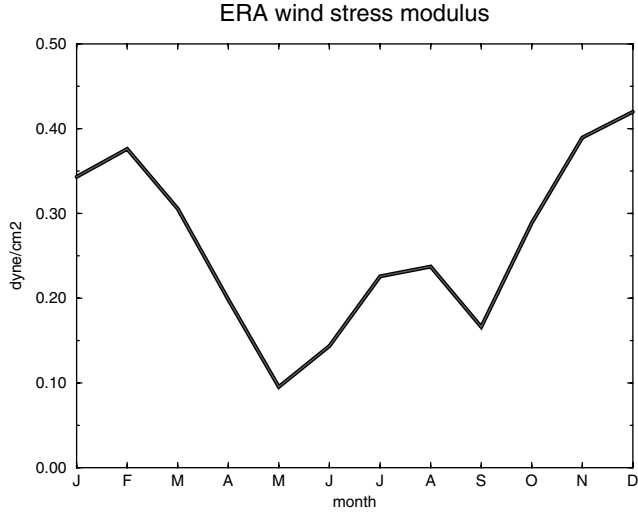


Figure 6. Annual cycle of the ECMWF reanalysis wind stress magnitude. Units are dyne cm^{-2} .

tion areas) are maximal in November–December. These are values in good agreement with previous estimates of the Adriatic Sea heat budget (see A97a). The seasonally averaged surface heat fluxes obtained by utilizing the ECMWF reanalysis data are shown in Figure 8. They illustrate the strong heat losses affecting the whole basin in winter and autumn (particularly over the northern Adriatic and along the eastern Adriatic coast) and the heat gains (except for the northern Adriatic basin) in spring and summer, particularly intense over the southern Adriatic. Despite the similarity of the computed basin-averaged heat fluxes the ECMWF analysis surface heat fluxes (not shown) are different from Figure 8 especially in the tendency to develop stronger gradients along the western coast rather than along the eastern one.

[27] In the model the solar radiation Q_s penetrates the water column. The transmission Tr and attenuation coefficient λ values reported in Table 1 were chosen according to *Jerlov* [1976]. The quantity

$$R_s = Q_s Tr e^{(\lambda z)} \quad (7)$$

is added to the heat equation as $\partial R_s / \partial z$ to propagate heat downward by radiative processes. Preliminary model tests indicated that the imposition of the winter heat fluxes was causing an excessive cooling in a (limited) part of the northern Adriatic basin. Therefore we added a heat flux correction term to the surface boundary condition for temperature, which took the following form:

$$K_H \left(\frac{\partial T}{\partial z} \right)_{z=\eta} = (\rho C_p)^{-1} [(1 - Tr)Q_s - Q_b - Q_h - Q_e + \left(\frac{\partial T}{\partial z} \right) (T_{z=0}^* - T_{z=\eta})]. \quad (8)$$

[28] The last term in (8) is the heat flux correction term, where $\partial Q / \partial T$ has been chosen to be $40 \text{ W m}^{-2} \text{ C}^{-1}$ [Oberhübler, 1988], $T_{z=\eta}$ is the model-predicted SST, and $T_{z=0}^*$ is the seasonally varying climatological SST of Figure 3. In this way the heat flux was forced to produce SSTs consistent with the seasonal climatology.

[29] The surface freshwater flux translates in a surface salinity flux W_s of the kind

$$W_s = (E - P - R)S_{z=\eta} \quad (9)$$

is composed by the balance of evaporation E , precipitation P , and river runoff ($R \neq 0$ at the “estuary” grid points only), while $S_{z=\eta}$ is the model-predicted surface salinity field. Monthly varying evaporation was computed from the latent heat flux according to

$$E = Q_e / L_E. \quad (10)$$

Monthly precipitation data were obtained from the *Legates and Wilmott* [1990] global 0.5° precipitation data set, as the ECMWF precipitation data resulted unrealistically low.

[30] The fresh water budget due to $(E - P)$ only is shown in Figure 9 for the basin average. As already described by A97a and *Raicich* [1996], the annual mean is approximately zero. Only if river runoff is used, the budget becomes negative as for a dilution basin. Seasonal fields of $(E - P)$ obtained utilizing

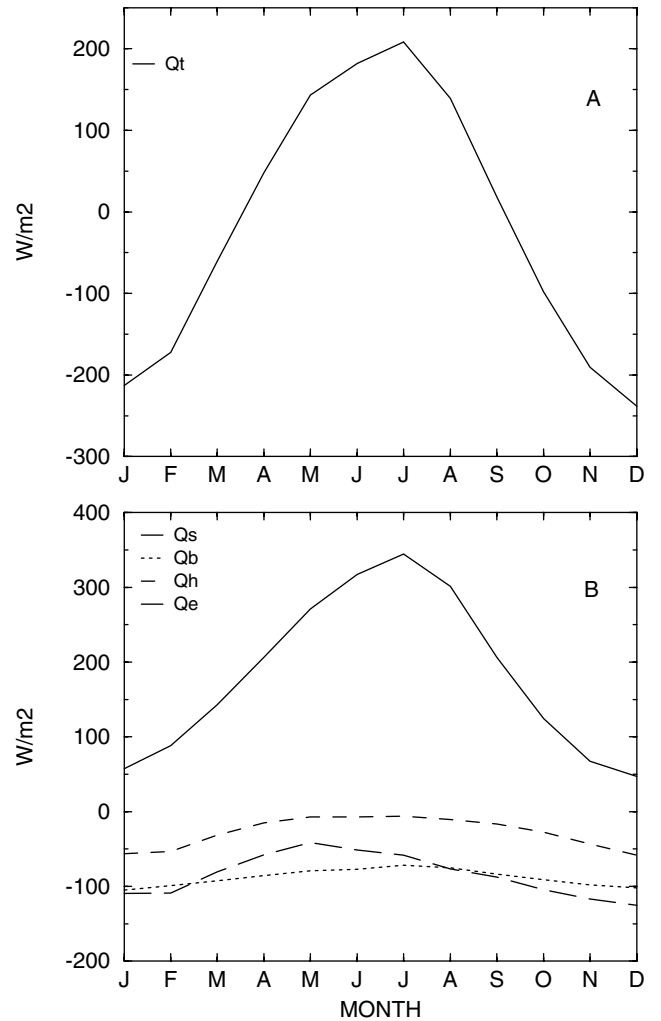


Figure 7. Annual cycle of the surface heat flux obtained from ECMWF reanalysis atmospheric data and *Reynolds* [1988] SST: (a) annual cycle of the total heat flux and (b) annual cycle of the heat flux components. Units are W m^{-2} .

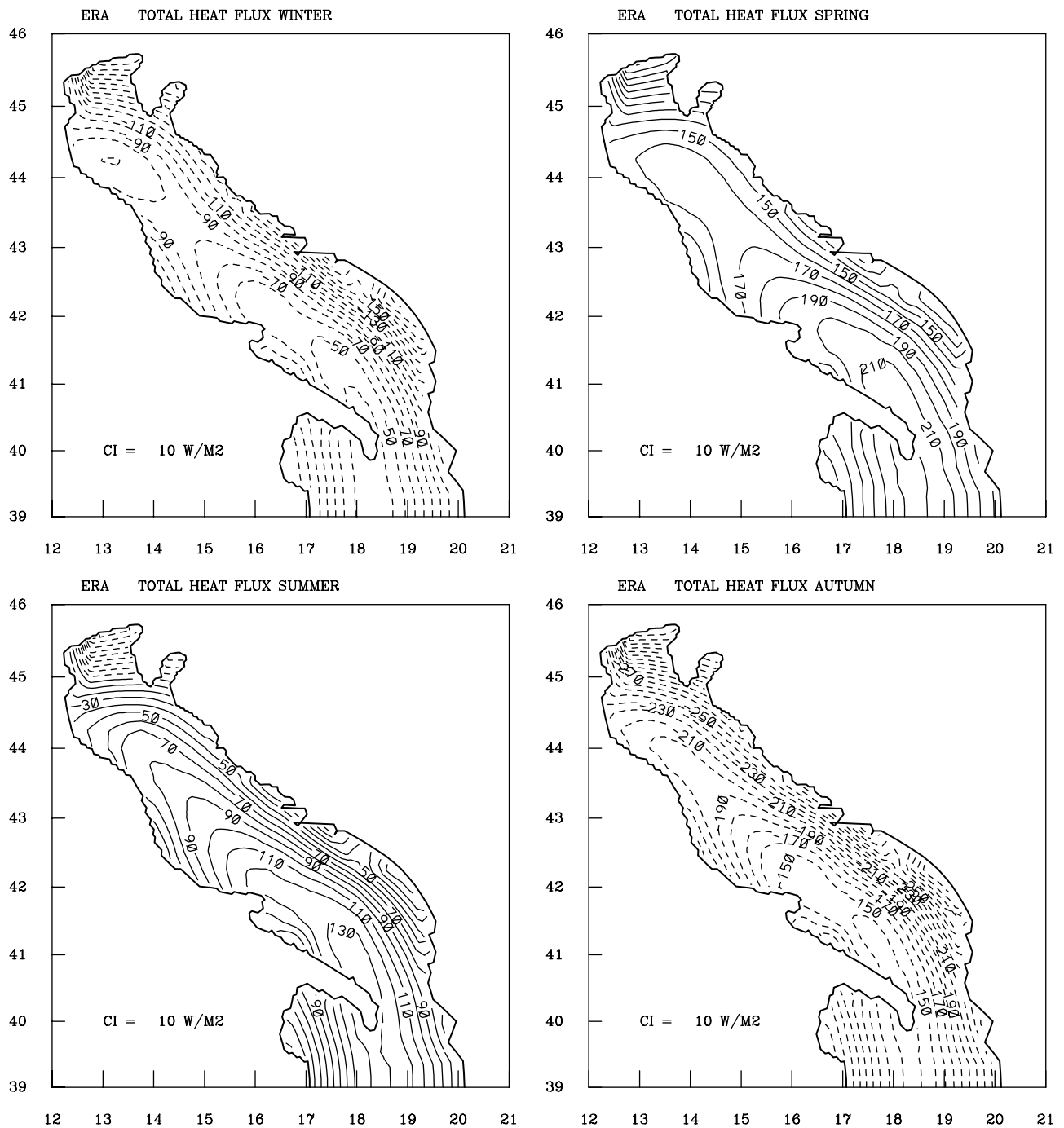


Figure 8. Seasonal climatological surface heat fluxes from the ECMWF reanalysis interpolated onto the curvilinear grid: (a) winter, (b) spring, (c) summer, and (d) autumn. The contour interval is 10 W m^{-2} .

the ECMWF reanalysis latent heat fluxes are shown in Figure 10. Noticable is the $E-P$ minimum in the southern Croatian-Albanian area; ($E-P$) fields obtained from the ECMWF analysis (not shown) differ from these fields mostly in their tendency to have stronger spatial gradients along the western coast rather than along the eastern one.

[31] The monthly river runoff data used were obtained from the Raicich [1994a, 1996] monthly climatology relative to the freshwater sources discharging into the basin. Figure 11 shows the runoff time series relative to the total runoff, the Po river

runoff, and the runoff relative to the northern, western (Po river runoff excluded), and eastern Adriatic coasts. The total runoff annual cycle shows two peaks, one in spring (due to snow melting from the Alps and the mountain ridges surrounding the basin) and one in late fall (due to heavy autumn rains). The northern, western, and eastern Adriatic rivers are not considered point sources in the model, but a distributed source function is imposed all along the shaded regions shown in Figure 1. Only the Po River is point like, and its contribution is distributed over six grid points in the horizontal.

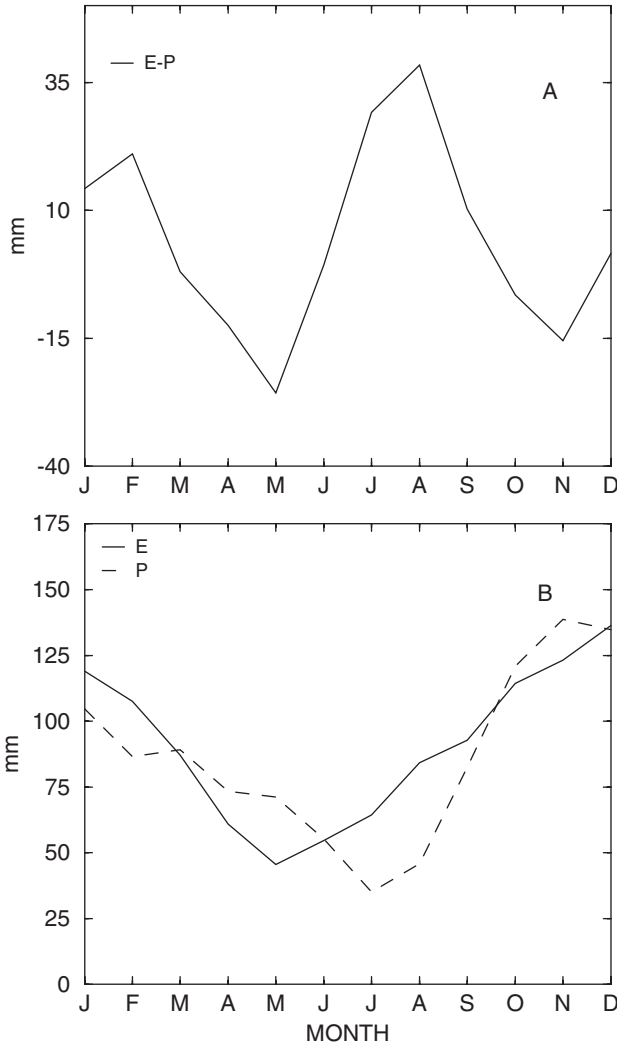


Figure 9. Annual cycle of the freshwater flux obtained from the ERA atmospheric data and the *Legates and Wilmott* [1990] precipitation data: (a): annual cycle of the total freshwater flux ($E-P$) and (b) annual cycle of E and P . Units are mm

[32] The annual mean water budget obtained from the ($E-P-R$) gives a gain of 1.18 m yr^{-1} , when using the ECMWF analysis derived evaporation, and to 0.85 m yr^{-1} , when the ECMWF reanalysis is used. The *Raichich* [1996] estimate of the freshwater budget ranges between 0.65 and 1.10 m yr^{-1} .

[33] Similarly to the heat flux, the salinity flux required a flux correction term in order to impose that water flux produces sea surface salinities consistent with the seasonal climatology. Therefore the surface boundary condition for salinity took the form

$$K_H \left(\frac{\partial S}{\partial z} \right)_{z=\eta} = W_s + \left(\frac{\Delta \sigma_1 H}{\gamma} \right) (S_{z=0}^* - S_{z=\eta}). \quad (11)$$

The last term in (11) is the salinity flux correction, where $S_{z=0}^*$ is the seasonal climatological surface salinity of Figure 4 and $\Delta \sigma_1 H$ is the thickness of the surface layer. The relaxation time γ has been chosen equal to 2.5 days. All the monthly forcing fields (Q , W_s , τ) were linearly interpolated between adjacent months. T^* and S^* were instead linearly interpolated between adjacent seasons.

[34] At the bottom, adiabatic boundary conditions are applied for temperature and salinity. For velocity a quadratic bottom drag coefficient is computed utilizing a logarithmic drag law coefficient and the bottom roughness length indicated in Table 1.

2.5. Lateral Open Boundary Conditions

[35] In order to specify open boundary conditions we developed a simple kind of “off-line” model nesting. Monthly varying temperature, salinity, and velocity data on the Adriatic model open boundary were obtained from the MOM 0.25° horizontal resolution simulation of the Mediterranean Sea general circulation [*Castellari*, 1996]. The same data were used to produce the seasonal climatologies of Figures 3 and 4, used as the initial and surface boundary conditions.

[36] Velocities normal to the boundary were directly specified from the large-scale MOM simulation monthly values, ensuring at each time step a zero net volume transport on the boundary. Moreover, since MOM is a rigid lid model and POM has a free surface, we imposed at each time step (in order to conserve volume)

$$U = [H / (\eta + H)] U_{\text{MOM}}, \quad (12)$$

where U is the vertically integrated velocity on the boundary, H is the bottom depth, η is the free-surface elevation, and U_{MOM} is the prescribed vertical integral of the velocity on the boundary from MOM.

[37] Tangential velocities were set to zero, as model tests indicated that the addition of the tangential velocities had a negligible effect on the model. Temperature and salinity on the outflow are locally upwinded, while if there is inflow, they are prescribed from the MOM monthly values. The open boundary data were applied to the model with a procedure analogue to that used for the atmospheric forcing functions (linear interpolation between adjacent months).

2.6. Numerical Experiments

[38] We carried out both diagnostic and prognostic experiments. The diagnostic experiments used the seasonal climatologies for temperature and salinity data from ATOSMOM as well as seasonally averaged wind stress fields from the ECMWF reanalysis data. The characteristics of the diagnostic experiments are summarized in Table 3. At each model time step the temperature and salinity fields were imposed to be equal to the initial field, utilizing the procedure used by *Mellor et al.* [1982] to diagnose the Atlantic Ocean circulation from temperature and salinity data. The prognostic experiments were run by utilizing the two different surface forcing functions (ECMWF analysis or reanalysis), and their characteristics are summarized in Table 4.

3. Diagnostic Calculations

[39] The diagnostic calculations can provide a first assessment of the seasonal circulation in terms of velocity field. Furthermore, by comparing the model results with the data analysis of A97b we can extract the role of the wind in setting the characteristics of the Adriatic Sea general circulation. In general, the simulation results confirm the seasonal character of many of the circulation patterns identified by A97b but shows also differences, particularly in winter and summer.

[40] In all diagnostic experiments a steady state was reached after about 5 days. The runs lasted for 10 days, and the results are shown in term of averages of the last 5 days of simulation.

[41] In Figure 12 the computed near-surface circulation is illustrated as trajectories computed as if the flow were steady

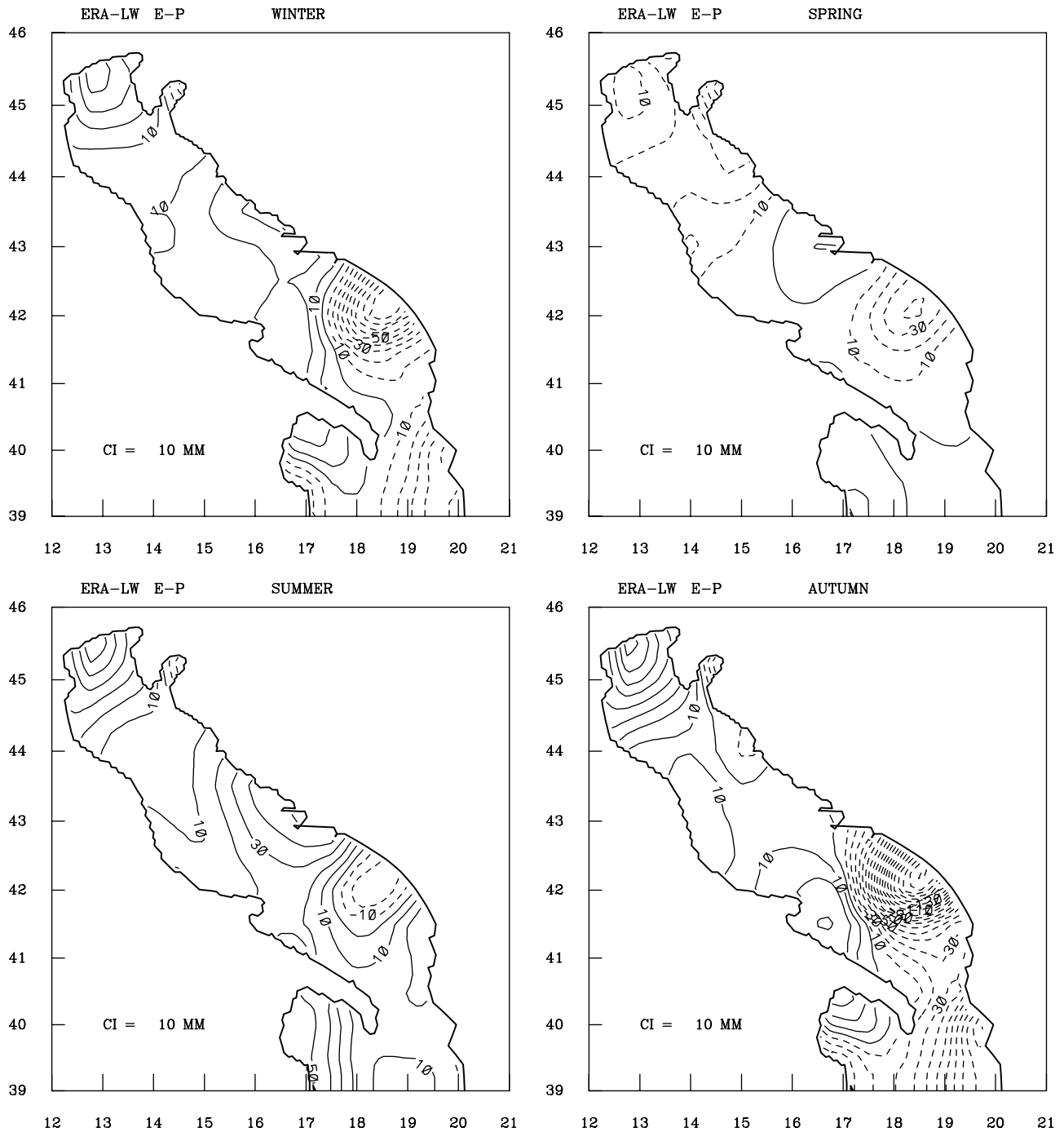


Figure 10. Seasonal climatological ($E-P$) fields obtained utilizing the ECMWF reanalysis data for the computation of evaporation: (a) winter, (b) spring, (c) summer, and (d) autumn. Fields are interpolated onto the curvilinear grid. The contour interval is $10 \text{ mm} (\text{month})^{-1}$.

for 5 days. The winter near-surface circulation (Figure 12a) shows a cyclonic circulation in the southern and central Adriatic and the presence of a well-developed WACC in the total velocity field. During winter, A97b could not detect a well-developed WACC in the dynamic height gradients, and they argued that the absence of the coastal current was due to density compensation processes. This process consists of a partial compensation of temperature and salinity gradients in the density field, resulting in the absence of a density-driven

current (baroclinic contribution) during winter. They argued that the WACC in this season should have a strong barotropic, wind-driven nature. Our simulations confirm that during winter the WACC is mainly wind-driven. In fact, if we compare the surface total velocity field of Figure 12a with its baroclinic component, shown in Figure 12b, it is evident that the WACC baroclinic structure is weak. Model-computed free-surface elevation (not shown) reveals that the maximum cross-shore pressure gradient is, indeed, at the northern part of

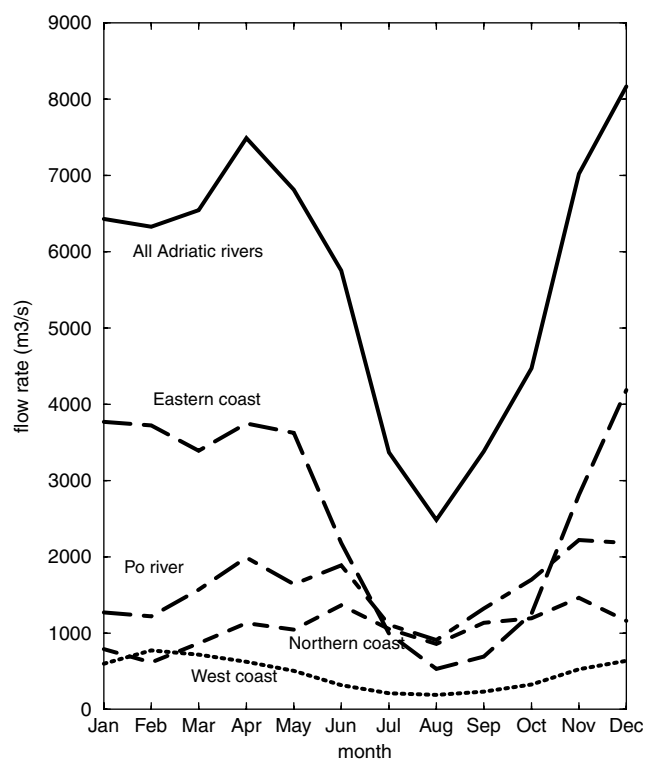


Figure 11. Time series of the Adriatic Sea river runoff. Redrawn from Raicich [1994a]. The annual cycle of the western coast runoff excludes the Po River contribution.

the west Adriatic coast at all seasons. During winter, when vertical homogeneous conditions are attained, the wind builds up a southward intense WACC determined by two combined effects: (1) a coastal current due to sea level buildup against the coast and coastal trapped waves that can generate a southward current (Kelvin waves generated along the coast can propagate southward, and they may counterbalance the upwelling favorable components of the wind stress.) and (2) a vorticity-induced functional boundary current due to positive wind stress curl. In fact, wind stress curl computations carried out using both the analysis and reanalysis wind stress fields (not shown) indicate, at all seasons, a positive wind stress curl in the WACC region. Thus, in this complicated sense the WACC is wind-driven during winter. The wind role in determining the southward flow of the WACC during winter is also highlighted by the baroclinic velocity field of Figure 12b, which shows a large-scale northward jet in the middle and southern Adriatic Sea that is not intensified along the eastern boundary. At the same time the SAd cyclonic gyre is weak and almost absent. This is also in partial agreement with the dynamic height computations of A97b.

[42] During summer the diagnostic simulation (Figure 13a) shows a WACC with large meanders. The correspondent model baroclinic velocity (Figure 13b) indicates that the meandering has a large baroclinic component. The WACC meanders appear in the same regions where A97b found that the WACC was broken in segments between the northern and central southern regions. We believe now that the WACC segments are in fact WACC meander pieces not well represented by the data distribution.

[43] Another interesting feature appearing in winter (Figure 12a), summer (Figure 13a), and autumn (not shown) is the presence of the NAd cyclonic gyre. A97b detected this feature

only in autumn, while P01 observed it in all seasons except winter. The diagnostic simulation indicates that during winter the NAd gyre has a clear barotropic, wind-driven structure, while in summer (Figure 13b) it has also a significant baroclinic component that strengthens during autumn. During summer and spring (not shown) both the WACC and the NAd gyre are mainly baroclinic. The WACC is mainly due to the strong cross-shore salinity frontal system, which is not compensated by a temperature front.

[44] In the southern Adriatic the summer current field appears to be broken into several smaller and mostly cyclonic gyres, a pattern consistent with the data-derived baroclinic picture of A97b. In all the seasons the Otranto Channel appears to be occupied by the border of an anticyclonic gyre on the eastern coast, determining a local recirculation.

[45] At 75 m depth the seasonal circulation shows for winter (Figure 14a), spring, and autumn (not shown) a WACC interacting with the MAd and SAd gyres. The ESAdC has a well-defined path in winter, while in the other seasons it is not present and is replaced by several small cyclonic circuits. This is different from the baroclinic picture of A97b, where the ESAdC appears to be present also in summer. During summer (Figure 14b), like the surface circulation, the southern Adriatic gyre is broken into smaller gyres. At this depth the Otranto Channel is clearly occupied in winter, spring, and autumn by an anticyclonic gyre to the north and a cyclonic gyre to the south of the strait. The anticyclonic gyre determines local recirculation and affects the inflow from the Ionian Sea. During summer the anticyclonic gyre weakens, while the cyclonic one strengthens.

4. Prognostic Calculations

[46] As a further step into the analysis of the seasonal variability of the general circulation of the Adriatic Sea, we describe now the simulations carried out utilizing the complete sets of forcing functions described in section 3. We recall (see Table 4) that the numerical experiments were performed with two kinds of forcing functions, obtained from ECMWF 1000 hPa analysis and ECMWF reanalysis. Both simulations produced circulation patterns similar to the observed climatology but with relevant differences resulting from the intrinsic deficiencies of both forcing data sets. We believe (see below) that both experiments can be regarded as two equally valid solutions of the Adriatic Sea general circulation problem.

[47] The total kinetic energy time series for the 3 year ADRI-N simulation is shown in Figure 15 and indicates that the model after the first year of integration acquired a repeating seasonal cycle. The same occurred for experiment ADRI-H.

[48] Seasonal averages of the surface circulation obtained from experiments ADRI-H and ADRI-N are shown in Figures 16 (winter) and 17 (summer), respectively. The immediate difference that can be noted between the two experiments is the larger-amplitude seasonal variability of the ADRI-N results with respect to ADRI-H and the more energetic circulation in

Table 3. Diagnostic Experiments Characteristics^a

Experiment	<i>T</i> and <i>S</i> Fields	Wind Stress
DIAGN-1	ATOSMOM winter	reanalysis: winter climatology
DIAGN-2	ATOSMOM spring	reanalysis: spring climatology
DIAGN-3	ATOSMOM summer	reanalysis: summer climatology
DIAGN-4	ATOSMOM autumn	reanalysis: autumn climatology

^aReanalysis: ECMWF surface reanalysis corrected by the 1.5 factor as proposed by Cavaleri and Bertotti [1997].

Table 4. Main Characteristics of the Prognostic Experiments^a

Experiment	<i>T</i> and <i>S</i> Initial Conditions	Wind Stress	Heat Flux	Evaporation
ADRI-H	winter	analysis	analysis	analysis
ADRI-N	winter	reanalysis	reanalysis	reanalysis

^a Analysis, heat flux, wind stress, and evaporation computed from the ECMWF 1000 hPa analysis parameters; reanalysis, heat flux, wind stress, and evaporation computed from the ECMWF surface reanalysis. The *Legates and Wilmott* [1990] precipitation data and the *Raichich* [1994a, 1996] runoff data were used in all the experiments.

ADRI-H. The latter is a direct consequence of the larger wind amplitude in the ECMWF analysis. With respect to winter (Figure 16), common features to both experiments are the well-developed WACC and ESAdC, both extending along almost the whole western and eastern coasts, respectively, and the cyclonic circulation in the southern Adriatic Sea. The occurrence of basin-wide coastal currents determines the connection of the circulation in the three major Adriatic subbasins. The WACC structure is basically invariant in ADRI-H, while in experiment ADRI-N both the WACC and the ESAdC exhibit a strong seasonal variability.

[49] In experiment ADRI-N the ESAdC in summer does not extend into the northern Adriatic Sea and affects only the southern Adriatic circulation. However, the diagnostic computations show the absence of the ESAdC in summer, not only a weakening.

[50] In both experiments the northern Adriatic circulation is generally cyclonic, but in experiment ADRI-N, like the diagnostic computations, a closed cyclonic gyre appears, comparable to the NAd gyre identified by A97b, P01, and our diagnostic calculations shown in Figures 12 and 13.

[51] The middle Adriatic is the region showing larger differences between ADRI-N and ADRI-H. Results from experiment

ADRI-H indicate the development of a well-defined and intense MAd gyre trapped between the WACC and the ESAdC and centered above the Pomo pits. It is persistent throughout the year, undergoing a certain degree of seasonal variability as its shape changes from season to season. The ADRI-N simulation did not produce the MAd gyre in winter, making only a relatively weak cyclonic circulation in spring (Figure 18). With respect to the diagnostic computations the velocity field in the central Adriatic is much smoother during winter and summer. This is due to the differences in thermohaline forcing that we will analyze later.

[52] In the southern Adriatic both simulations indicated a persistent cyclonic circulation in all the seasons. This is in agreement with P01 but very different from the diagnostic simulations where, particularly during summer (see Figure 12a), the resulting circulation was composed of small cyclonic and anticyclonic circuits. The seasonality appears more pronounced in experiment ADRI-N (Figures 16b and 17b). A clear connection of the SAd gyre with the Ionian Sea inflow appears only in winter, while in the other seasons the region of the Otranto Channel shows a general outflow, turning around the southern tip of Apulia, connected with the surface WACC. Our results agree with the findings of P01 since both

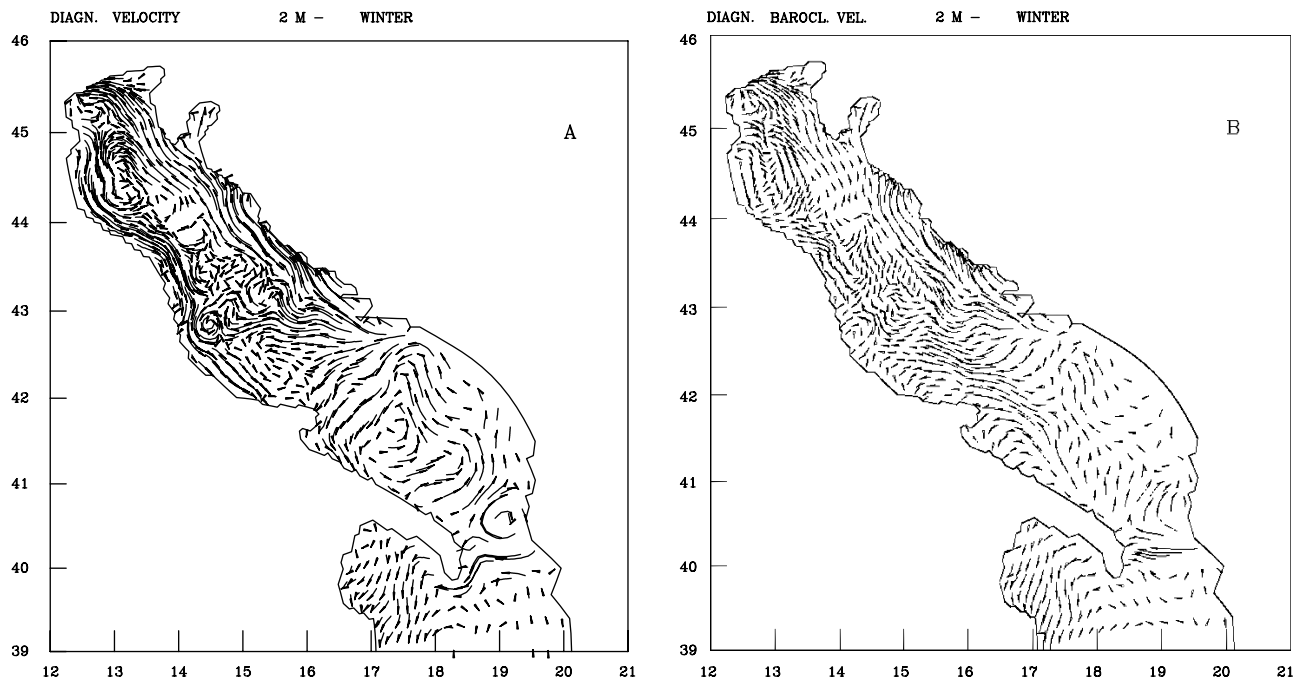


Figure 12. Diagnostic simulations. Winter velocity trajectories at 2 m depth computed as if the flow were steady for 5 days: (a) total velocity and (b) baroclinic component of the velocity field. Not all the grid points have been plotted.

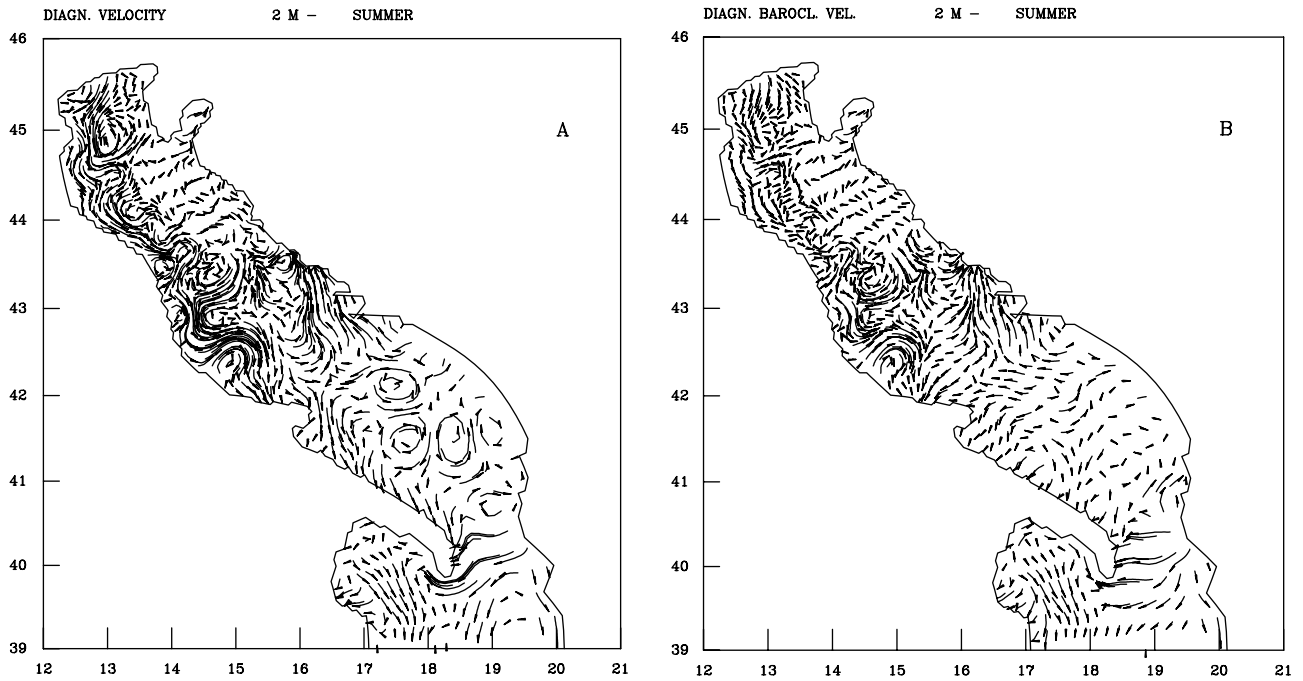


Figure 13. As in Figure 12 but for summer.

solutions show a shift of the maximum intensity of the WACC offshore during summer.

[53] The circulation at 75 m depth obtained in the two experiments ADRI-H and ADRI-N is shown in Figures 19 and 20 for winter and summer, respectively. The ADRI-H circulation appears more intense as a consequence of the stronger forcing functions imposed at the surface. The MAD and SAd gyres in the central and southern subbasins are strongly connected in winter (Figure 19a)

and spring (not shown), while in summer (Figure 20) the connection undergoes a relative weakening, to strengthen again in summer.

[54] Part of the reasons for the different circulation in the ADRI-H and ADRI-N experiments can be ascribed to the differences in the thermohaline structure of the simulations. In order to explain this we proceed to describe the spatial distribution of the hydrological properties as simulated by the

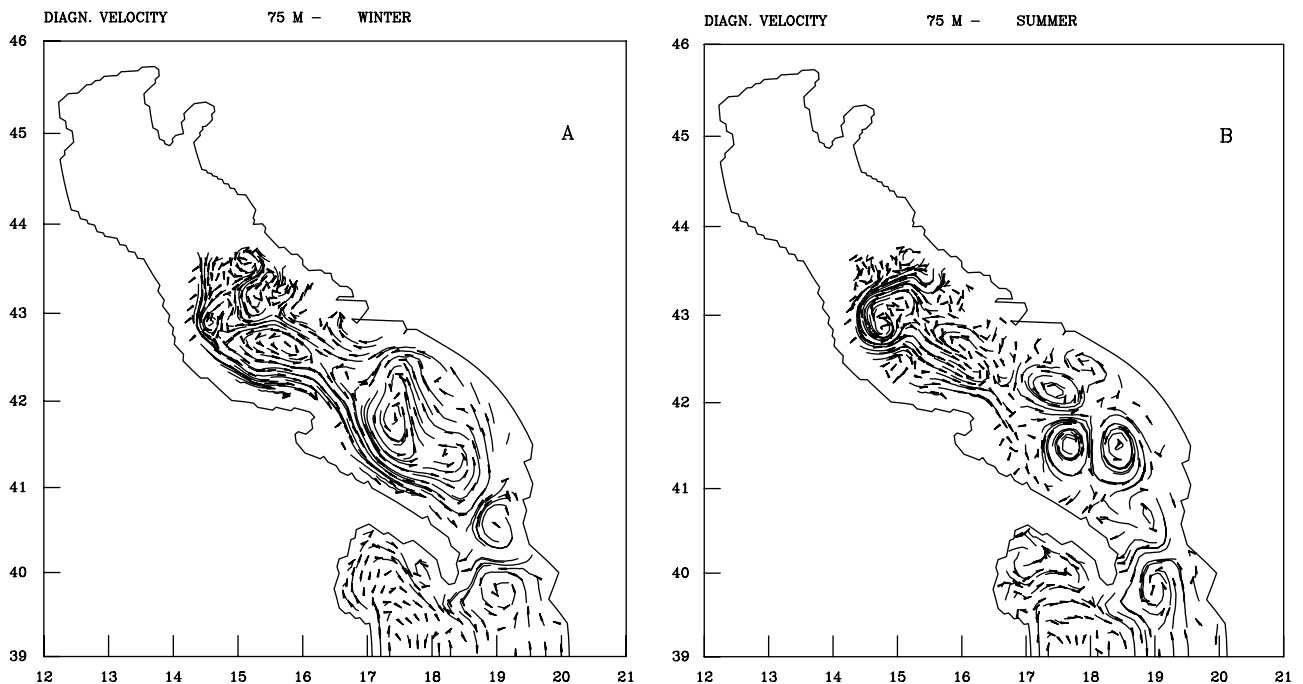


Figure 14. Diagnostic simulations. Velocity trajectories at 75 m depth computed as if the flow were steady for 10 days: (a) winter and (b) summer. Not all the grid points have been plotted.

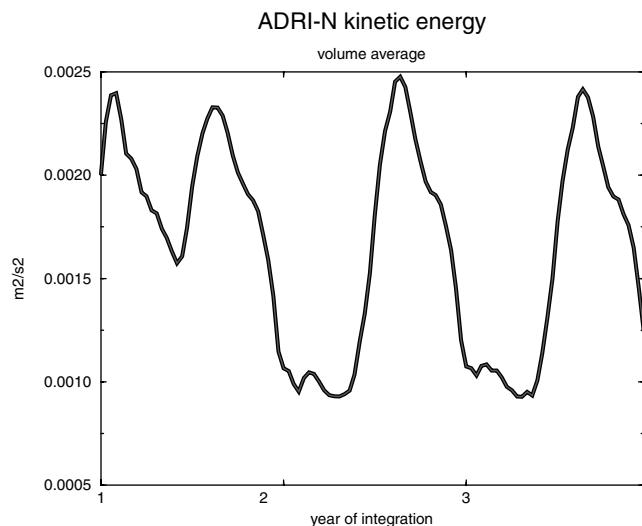


Figure 15. Time series of the model basin averaged kinetic energy.

two experiments. Winter and summer temperature fields for the two prognostic experiments performed are shown in Figures 21 and 22, respectively. The comparison with the seasonal climatology of Figures 3 and 4 shows a relatively good agreement with data. The simulations show a cold northern Adriatic surface water area extending southward along almost the entire western Adriatic coast, in the region of the WACC path. We stress again that in such areas, temperature increases offshore, therefore determining a pressure gradient conflicting with the southward direction of the WACC.

However, temperatures are warmer than observations by 1° – 2° C everywhere. On the contrary, in summer (Figure 22) and autumn (not shown), simulated surface temperature are generally lower than the observations. In partial disagreement with the observations both experiments, but particularly ADRI-N, indicate for the summer (Figure 22) and the autumn (not shown) the development of a cold surface temperature front along the eastern coast of the southern Adriatic Sea. This feature is not present in the seasonal climatology of Figure 3 and indicates the occurrence of upwelling processes in the model simulations but not in the data.

[55] The simulated winter and summer surface salinity seasonal fields obtained by the two prognostic experiments are shown in Figures 23 and 24, respectively. Both simulations indicate that the salinity field is significantly controlled by the land-based freshwater inputs determined by the imposed river runoff. However, the distribution obtained by the two simulations indicates differences that should be ascribed to the different latent heat fluxes. ADRI-H indicates the tendency of the surface salinity flux to generate higher surface salinity values in the northern Adriatic (Figures 23a and 24a). This is particularly evident in summer (Figure 24a), where in disagreement with the observations the surface salinity in the northern Adriatic attains values higher than 38.2 psu, while observation indicates (A97b and Figure 4) a general freshening of the northern Adriatic surface waters. From the salinity point of view the results of experiment ADRI-N seem to offer a better simulation as the model correctly reproduces the progressive decrease of the salinity value from winter (Figure 23b) to summer (Figure 24b) in the northern Adriatic. A contribution to the freshening of the northern Adriatic is also given by the offshore extension of the low-salinity front, which is larger in ADRI-N than in ADRI-H.

[56] In order to quantify the differences between the two simulations with respect to the data we computed the root mean square (RMS) differences between the seasonally aver-

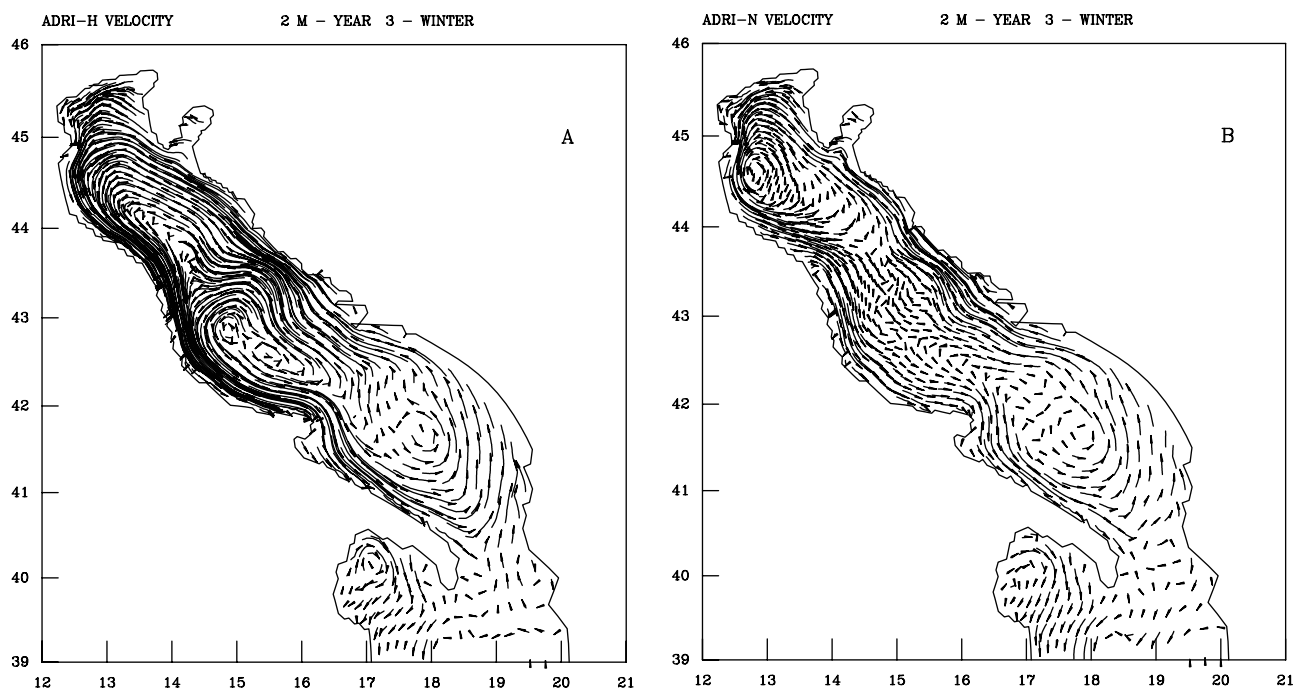


Figure 16. Prognostic simulations. Winter velocity trajectories at 2 m depth computed as if the flow were steady for 5 days: (a) ADRI-H and (b) ADRI-N. Not all the grid points have been plotted.

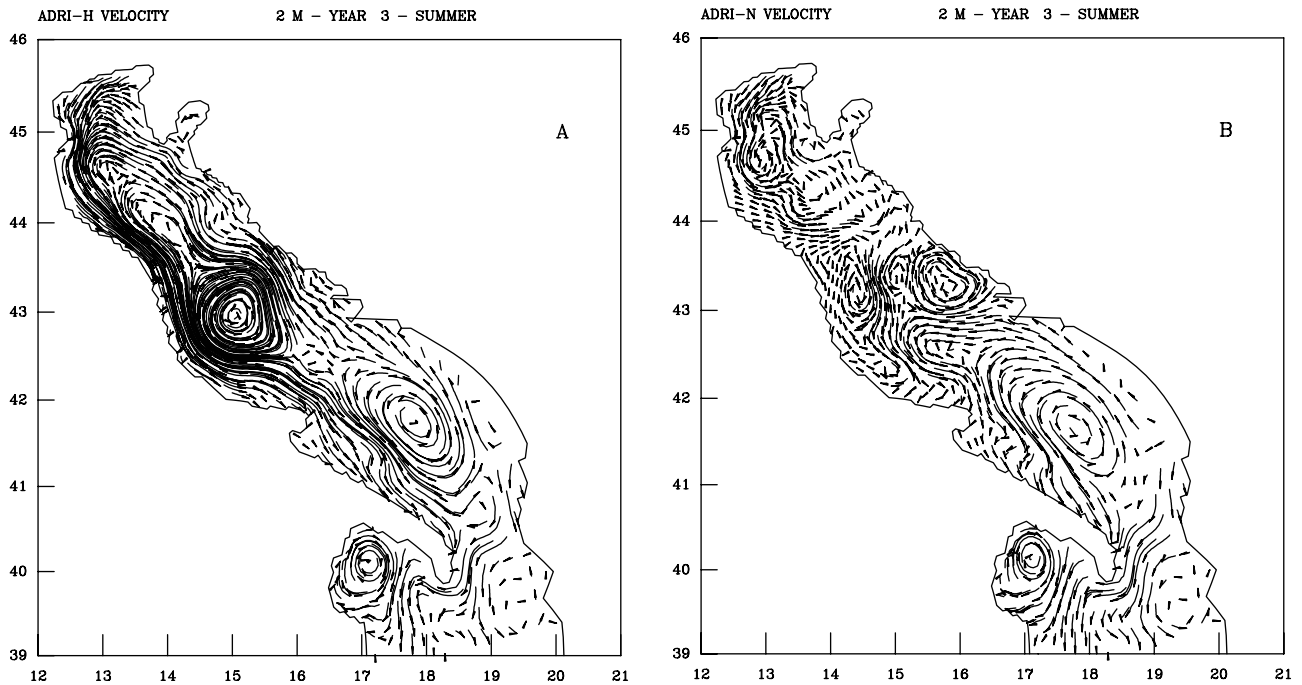


Figure 17. As in Figure 16 but for summer.

aged simulated temperature and salinity fields and the observed fields (Figures 3 and 4). Results of this computation are shown in Table 5.

[57] It can be seen that both simulations produced comparable RMS differences having approximately the same magnitude in all seasons, but ADRI-N has lower values except for the winter salinity. This, together with the larger amplitude of the seasonal cycle (in overall agreement with A97b and P01), leads us to conclude that ADRI-N is a better experiment even if we believe also that ADRI-H is a possible solution of the circulation problem in the Adriatic Sea.

5. Conclusions

[58] This paper has shown results obtained from diagnostic and prognostic simulations of the Adriatic Sea general circulation and its seasonal variability. The diagnostic simulations gave a first assessment of the general circulation within the limits of the diagnostic procedure used and the computation of gridded fields obtained from observations. These experiments gave the first definitive indication of the relative role of the wind versus thermohaline forcing in setting the circulation characteristics. In this respect an important finding concerns the role of the wind in sustaining the WACC in the northern Adriatic during winter. The results of the diagnostic simulations indicate that the WACC has a weak baroclinic velocity component in winter because of density compensation processes in the coastal areas. During summer the WACC forms wide meanders characterized by a significant baroclinic component, while the MAd and SAd gyres are broken into smaller-scale structures. Thus the WACC current system has a seasonal variability characterized by a large wind-driven component during winter and baroclinic meanders in the remaining months. A density compensation mechanism can be shown to be at work during winter, while during summer the salinity-driven, river runoff front is of paramount importance for the WACC structure and instability. In the second part of this paper we will investigate in depth the wind versus thermohaline forcing

importance and clarify the role played by the negative heat flux (acting to set an antiestuarine circulation) and the positive water flux (acting to set an estuarine circulation) in determining the winter characteristics of the WACC.

[59] The prognostic simulations used different atmospheric data sets to determine the seasonal circulation. The comparison

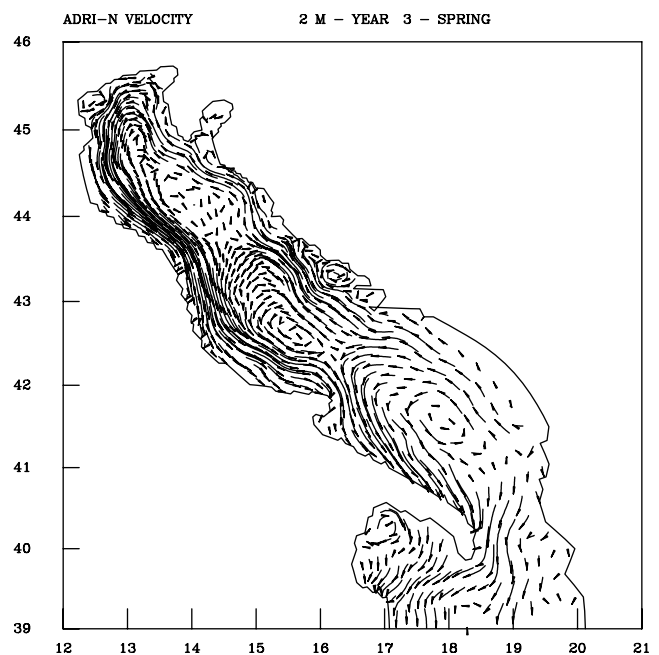


Figure 18. Experiment ADRI-N. Spring velocity trajectories at 2 m depth computed as if the flow were steady for 5 days. Not all the grid points have been plotted.

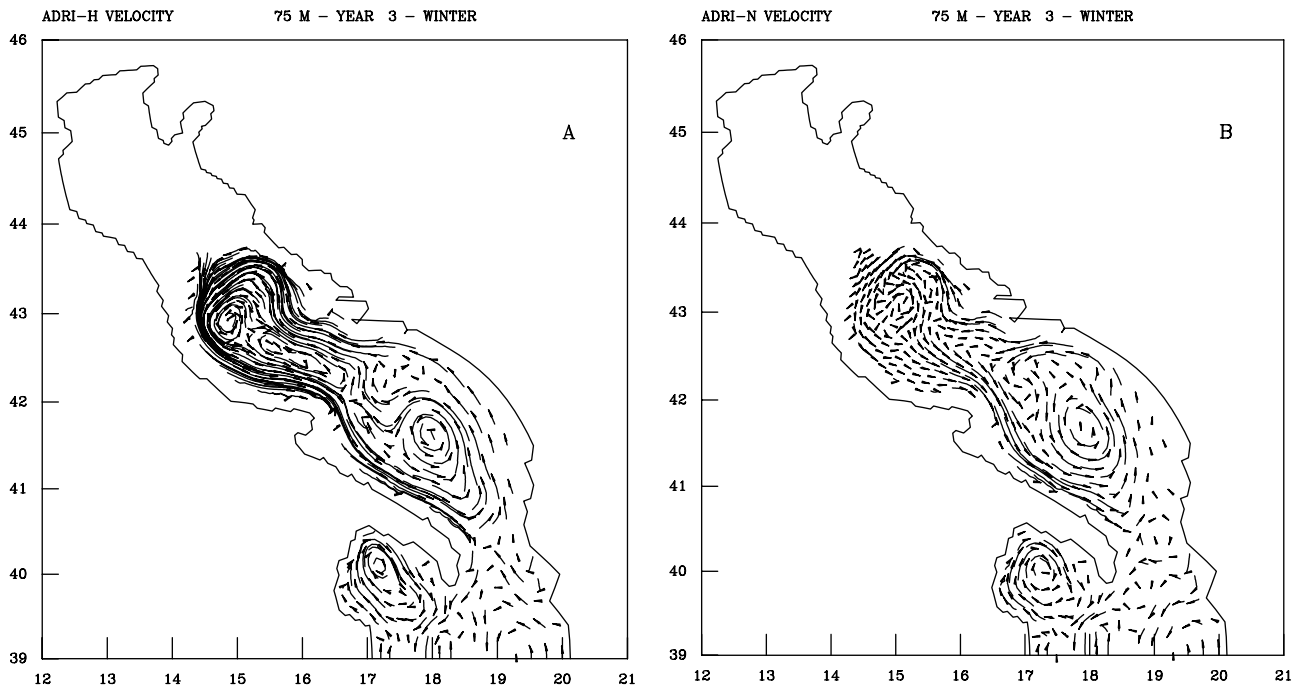


Figure 19. Prognostic simulations. Winter velocity trajectories at 75 m depth computed as if the flow were steady for 10 days: (a) ADRI-H and (b) ADRI-N. Not all the grid points have been plotted.

between the two experiments and the diagnostic calculations showed a relatively higher degree of similarity of the ADRI-N experiment with observations with respect to ADRI-H. This led us to conclude that in regional seas the ocean circulation is likely to be simulated better by using surface atmospheric parameters if ECMWF analyses have to be used. This could

not be the case for larger ocean areas as shown by *Rosati and Miyakoda* [1988].

[60] We can say that the differences are first due to the strength of the wind and second to the thermohaline forcing. The results of the two set of simulations seems to suggest that stronger wind stress does not only produce larger current

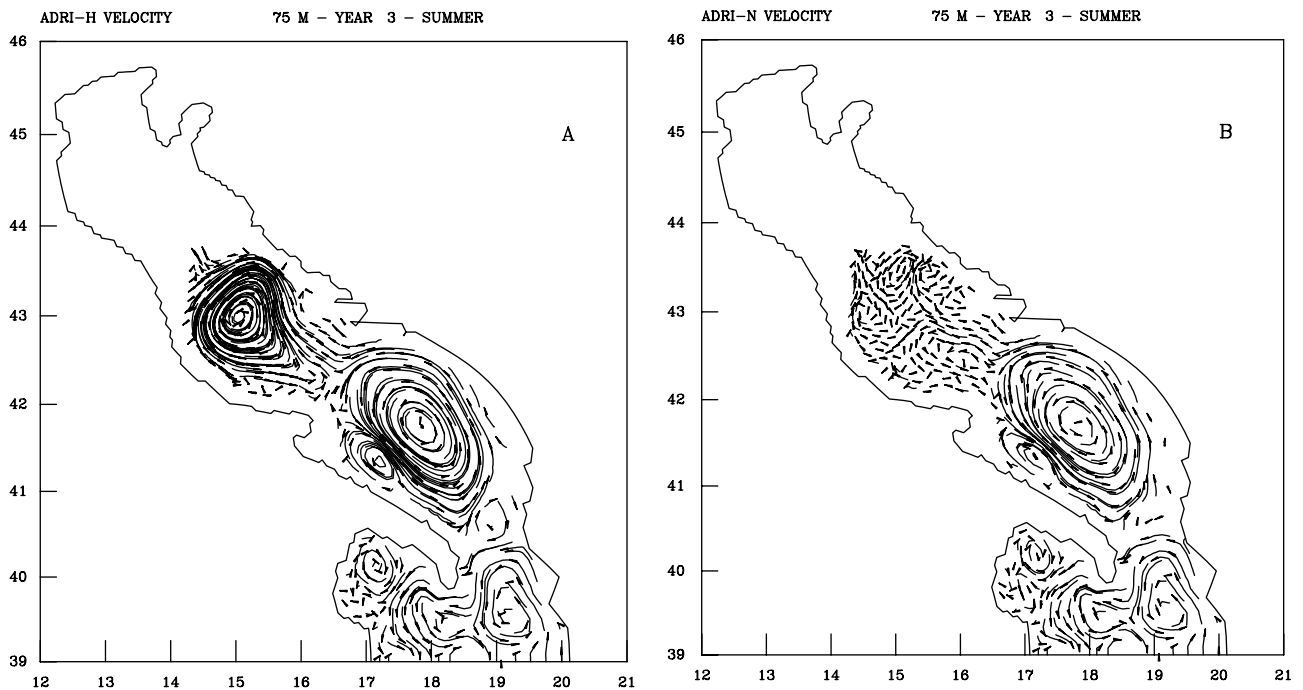


Figure 20. As in Figure 19 but for summer.

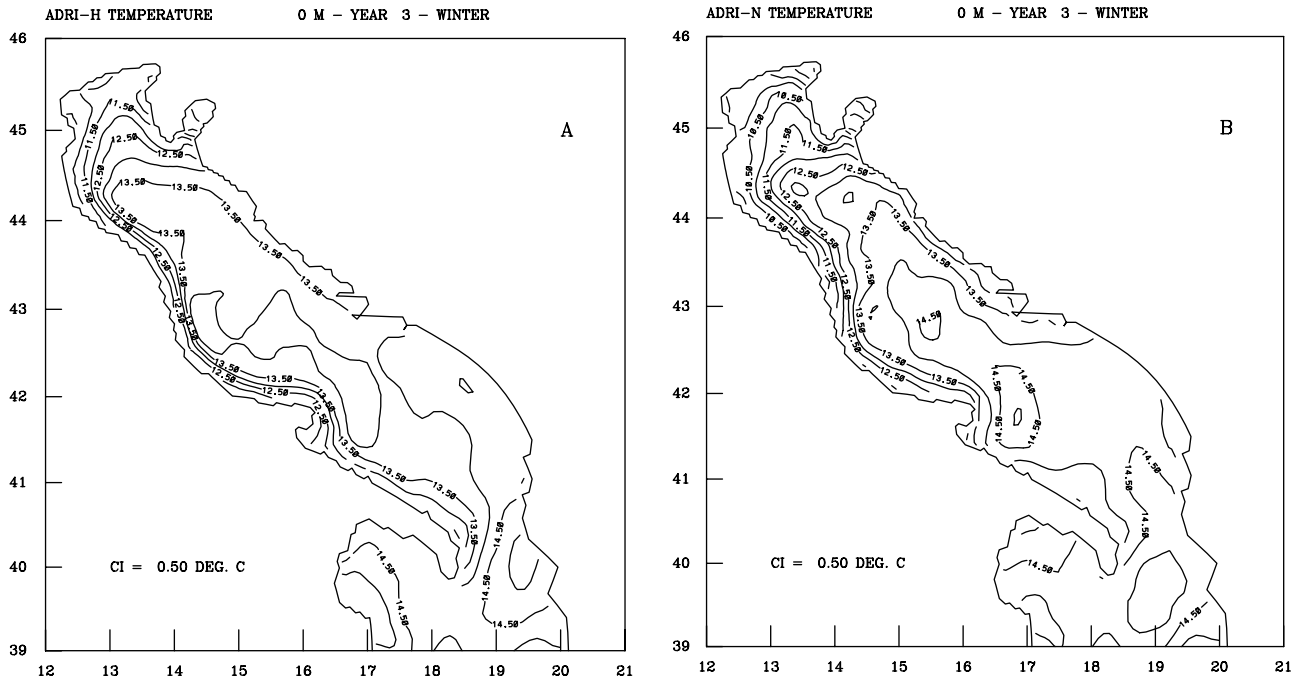


Figure 21. Prognostic simulations. Winter surface temperature distribution: (a) ADRI-H and (b) ADRI-N. The contour interval is 0.5°.

velocities but also influences the degree of seasonal variability of the circulation. ADRI-H produced an almost seasonally invariant general circulation, characterized in all seasons by the connection of the overall cyclonic circulation in the three major Adriatic subbasins by means of the two coastal currents (WACC and ESAdC). The WACC, in particular, does not

show much spatial variability through the seasons and persists throughout the year as a narrow coastal jet stretched against the western Adriatic coast. On the other hand, the use of a weaker wind stress forcing (ADRI-N) seems to increase the amplitude of the seasonal variability in the WACC and the ESAdC regions. In particular, the WACC in summer loses (in

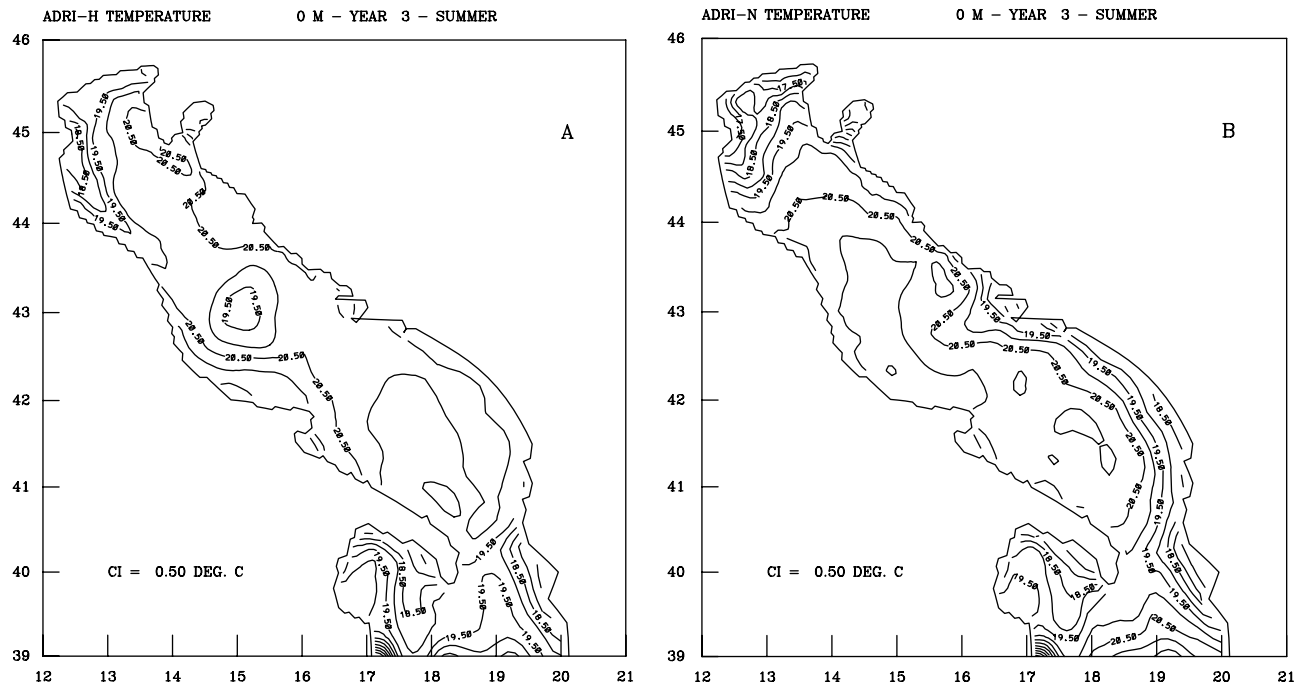


Figure 22. As in Figure 21 but for summer.

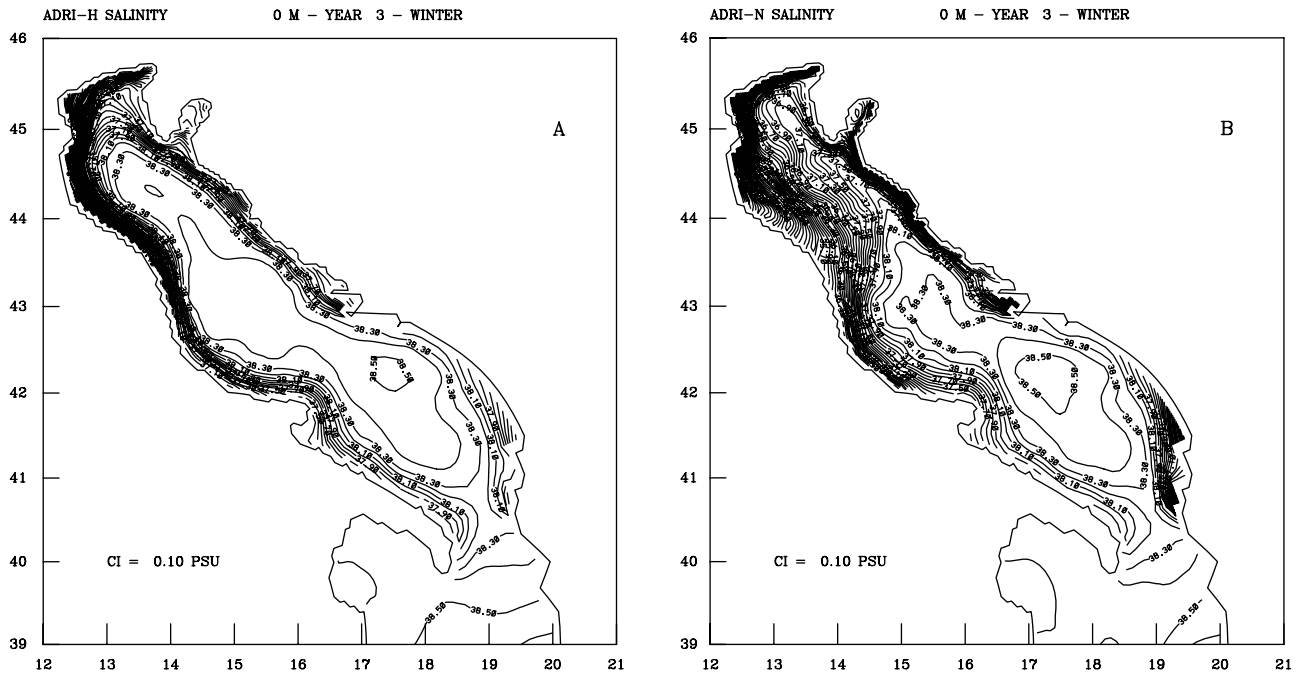


Figure 23. Prognostic simulations. Winter surface salinity distribution: (a) ADRI-H and (b) ADRI-N. The contour interval is 0.1 psu.

agreement with the observations of P01) its coastal jet characteristics and produces large meanders and anticyclonic gyres along the western coast.

[61] However, neither of the two simulations can be considered as entirely satisfactory as both simulations are

affected by some discrepancies with respect to known features of the Adriatic Sea circulation, the most notable being the almost complete absence of the MAD gyre in ADRI-N. We ascribe these discrepancies to the inherent limitations of the data used to compute the atmospheric forcing functions; in

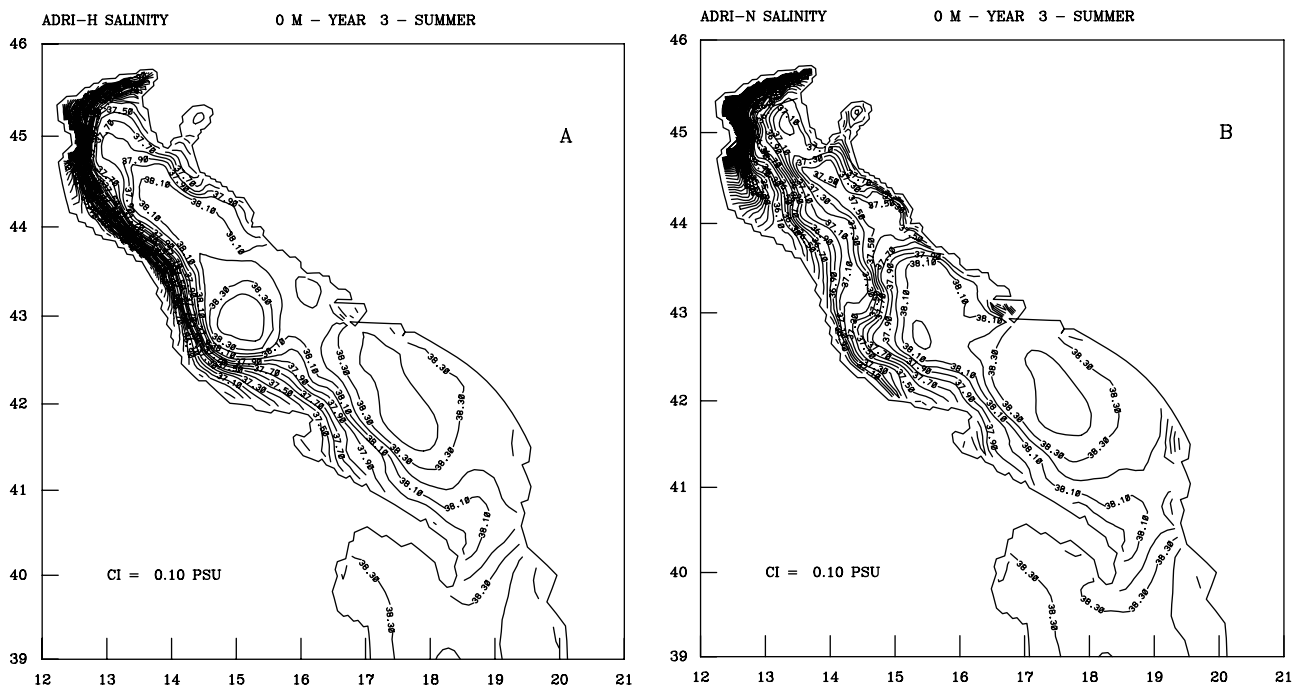


Figure 24. As in Figure 23 but for summer.

Table 5. Seasonal Temperature and Salinity RMS Differences Between the Simulated Seasonal Averages and the Correspondent Observed Fields

Experiment	Temperature, °C				Salinity, psu			
	Winter	Spring	Summer	Autumn	Winter	Spring	Summer	Autumn
ADRI-H	0.92	2.47	2.07	2.24	0.45	0.54	0.40	0.58
ADRI-N	0.73	1.61	1.99	2.16	0.65	0.51	0.46	0.38

particular, the spatial resolution of the atmospheric data is, even in the best case (ECMWF analysis), coarse with respect to the size of a small semienclosed basin such as the Adriatic Sea.

[62] **Acknowledgments.** This research has been undertaken in the framework of the Mediterranean Targeted Project II - MATER (MTP II-MATER) project. We acknowledge the support of the European Commission's Marine Science and Technology (MAST) program under contract MAS3-CT96-0051. This is MTP-II MATER publication 38. V. H. Kourafalou was supported by the European Union Human Capital and Mobility Program grant MAS2CT-94-5018. A. Maggiore was supported by the second phase of the MURST/CNR PRISMA program. The work had continuing support from the Mediterranean Forecasting System Pilot Project (MFSPP) (contract MAS3-CT97-0171) and by the ICRAM MAT Project. We thank L. Cavaleri, G. L. Mellor, and the anonymous reviewers for helpful criticisms and advice. We are indebted to L. Giacomelli for help in the manuscript editing.

References

- Artegiani, A., R. Azzolini, and E. Salusti, On the dense water in the Adriatic Sea, *Oceanol. Acta*, *12*, 151–160, 1989.
- Artegiani, A., D. Bregant, E. Paschini, N. Pinardi, F. Raicich, and A. Russo, The Adriatic Sea general circulation, part I, Air Sea interactions and water mass structure, *J. Phys. Oceanogr.*, *27*, 1492–1514, 1997a.
- Artegiani, A., D. Bregant, E. Paschini, N. Pinardi, F. Raicich, and A. Russo, The Adriatic Sea general circulation, part II, Baroclinic circulation structure, *J. Phys. Oceanogr.*, *27*, 1515–1532, 1997b.
- Bergamasco, A., and M. Gacic, Baroclinic response of the Adriatic Sea to an episode of Bora wind, *J. Phys. Oceanogr.*, *26*, 1354–1369, 1996.
- Blumberg, A. F., and G. L. Mellor, A description of a three-dimensional coastal ocean circulation model, in *Three-Dimensional Coastal Ocean Models*, *Coastal Estuarine Sci.* vol. 4, edited by N. S. Heaps, pp. 1–16, AGU, Washington, D. C., 1987.
- Bone, M., Development of a non-linear levels model application to Bora-driven circulation on the Adriatic shelf, *Estuarine Coastal Shelf Sci.*, *37*, 475–496, 1993.
- Castellari, S., A numerical study of water mass formation processes and seasonal to interannual variability in the Mediterranean Sea, Ph.D. thesis, 242 pp., Rosenstiel School of Mar. and Atmos. Sci., Univ. of Miami, Miami, Fla., 1996.
- Castellari, S., N. Pinardi, and K. Leaman, A model study of air-sea interactions in the Mediterranean Sea, *J. Mar. Syst.*, *18*, 89–114, 1998.
- Cavaleri, L., and L. Bertotti, In search of the correct wind and wave fields in a minor basin, *Mon. Weather Rev.*, *125*, 1964–1975, 1997.
- Cavaleri, L., A. Lavagnini, and S. Martorelli, The wind climatology of the Adriatic Sea deduced from coastal stations, *Nuovo Cimento Soc. Ital. Fis. C*, *19*, 37–50, 1996.
- Gibson, J. K., P. K. Kallberg, S. Uppala, A. Hernandez, A. Nomura, and E. Serrano, ERA description, *ECMWF Re-anal. Proj. Rep. Ser.1*, 72 pp., Reading, Engl., U.K., 1997.
- Hellerman, S., and M. Rosenstein, Normal monthly wind stress over the world ocean with error estimates, *J. Phys. Oceanogr.*, *13*, 1093–1104, 1983.
- Hopkins, T. S., A. Artigiani, C. Kinder, and A. Pariante, A discussion of the northern Adriatic circulation and flushing as determined by the ELNA hydrography, in *Ecosystem Research Report: The Adriatic Sea*, *EU Environ. Ser.*, vol. 32, pp. 87–106, Eur. Comm., Brussels, 1999.
- Jerlov, N. G., *Marine Optics*, 231 pp., Elsevier Sci., New York, 1976.
- Kondo, J., Air-sea bulk transfer coefficients in diabatic conditions, *Boundary Layer Meteorol.*, *9*, 91–112, 1975.
- Kourafalou, V. H., Process studies on the Po river plume, *J. Geophys. Res.*, *104*, 29,963–29,985, 1999.
- Kuzmic, M., Exploring the effects of Bura over the northern Adriatic: CZCS imagery and a mathematical model prediction, *Int. J. Remote Sens.*, *12*, 207–214, 1991.
- Legates, D. R., and C. J. Wilmott, Mean seasonal and spatial variability in a gauge corrected global precipitation, *Int. J. Climatol.*, *10*, 121–127, 1990.
- Maggiore, A., M. Zavatarelli, M. G. Angelucci, and N. Pinardi, Surface heat and water fluxes in the Adriatic Sea: Seasonal and interannual variability, *Phys. Chem. Earth*, *23*, 561–567, 1998.
- Malanotte Rizzoli, P., and A. Bergamasco, The dynamics of the coastal region of the northern Adriatic Sea, *J. Phys. Oceanogr.*, *13*, 1105–1130, 1983.
- May, P. W., Climatological flux estimates in the Mediterranean Sea, part I, Winds and wind stresses, *NORDA Tech. Rep.*, *54*, 58 pp., Nav. Oceanogr. and Atmos. Res. Lab., Stennis Space Cent., Miss., 1982.
- May, P. W., A brief explanation of Mediterranean heat and momentum flux calculations, *NORDA Code 322*, 5 pp., Nav. Oceanogr. and Atmos. Res. Lab., Stennis Space Cent., Miss., 1986.
- Mellor, G. L., An equation of state for numerical models of oceans and estuaries, *J. Atmos. Oceanic Technol.*, *8*, 609–611, 1991.
- Mellor, G. L., User's guide for a three-dimensional primitive equation, numerical ocean model, AOS program report, 34 pp., Princeton Univ., Princeton, N.J., 1998.
- Mellor, G. L., and A. F. Blumberg, Modeling vertical and horizontal diffusivities with a sigma coordinate system, *Mon. Weather Rev.*, *113*, 1279–1383, 1986.
- Mellor, G. L., and T. Yamada, Development of a turbulence closure sub-model for geophysical fluid problems, *Rev. Geophys.*, *20*, 851–875, 1982.
- Mellor, G. L., C. R. Mechoso, and E. Keto, A diagnostic calculation of the general circulation of the Atlantic Ocean, *Deep Sea Res., Part A*, *29*, 1171–1192, 1982.
- Miyakoda, K., and J. Sirutis, Comparative integrations of global models with various parameterized processes of subgrid-scale vertical transports, *Beitr. Phys. Atmos.*, *50*, 445–487, 1977.
- Oberhüber, J. M., The budgets of heat, buoyancy and turbulent kinetic energy at the surface of the global ocean: An atlas based on the COADS data set, *Max Planck Inst. Meteorol. Rep. 15*, 20 pp., Hamburg, Germany, 1988.
- Orlic, M., M. Kuzmic, and Z. Pasaric, Response of the Adriatic Sea to the Bora and Sirocco forcing, *Cont. Shelf Res.*, *14*, 91–116, 1994.
- Ovchinnikov, I. M., V. I. Zats, V. G. Krivosheya, M. S. Nemirovsky, and A. I. Udodov, Winter convection in the Adriatic and formation of deep eastern Mediterranean waters, *Ann. Geophys., Ser. B*, *5*, 89–92, 1987.
- Payne, R. E., Albedo of the sea surface, *J. Atmos. Sci.*, *29*, 959–970, 1972.
- Poulain, P. M., Adriatic Sea surface circulation as derived from drifter data between 1990 and 1999, *J. Mar. Syst.*, *29*, 3–32, 2001.
- Raicich, F., Note on flow rates of the Adriatic rivers, *Techn. Rep. RF02/94*, 8 pp., Ist. Talassografico Sperimentale Trieste, Trieste, Italy, 1994a.
- Raicich, F., Note on the precipitation on the Adriatic Sea coast, *Techn. Rep. RF03/94*, 6 pp., Ist. Talassografico Sperimentale Trieste, Trieste, Italy, 1994b.
- Raicich, F., On the fresh water balance of the Adriatic Sea, *J. Mar. Syst.*, *9*, 305–319, 1996.
- Reed, R. K., An evaluation of formulas for estimating clear sky insolation over the ocean, *NOAA-ERL 352-PMEL Tech. Rep. 26*, 25 pp., Natl. Oceanic and Atmos. Technol., Silver Spring, Md., 1975.
- Reed, R. K., On estimating insolation over the ocean, *J. Phys. Oceanogr.*, *17*, 854–871, 1977.
- Reynolds, R. W., A real time global sea surface temperature analysis, *J. Clim.*, *1*, 75–86, 1988.
- Rosati, A., and K. Miyakoda, A general circulation model for upper ocean simulation, *J. Phys. Oceanogr.*, *18*, 1601–1626, 1988.

- Roussenov, V., V. Artale, E. Stanev, and N. Pinardi, A seasonal model of the Mediterranean Sea circulation, *J. Geophys. Res.*, 100, 13,515–13,538, 1995.
- Schrimpf, W., W. Eifler, and T. Kupusovic, Barotropic simulation in the northern Adriatic during a Bura-wind episode by three different numerical models, in *Computer Methods in Water Resources II.*, vol. 2, *Computational Hydraulics and Hydrology*, edited by D. Ouazar, et al., pp. 377–392, Comput. Mech., Billerica, Mass., 1992.
- Smagorinsky, J., Some historical remarks on the use of nonlinear viscosities, in *Large Eddy Simulation of Complex Engineering and Geophysical Flows*, edited by B. Galperin, and S. A. Orszag, pp. 3–36, Cambridge Univ. Press, New York, 1993.
- Vested, H. J., P. Berg, and T. Uhrenholdt, Dense water formation in the northern Adriatic Sea, *J. Mar. Syst.*, 18, 135–160, 1998.
-
- V. H. Kourafalou, National Center for Marine Research Elliniko, Athens, 166-04 Greece. (vily@ismini.fl.ncmr.gr).
- A. Maggiore, Royal School of Mines, Imperial College, Prince Consort Road, London SW7 2BP, England, UK. (A.Maggiore@ic.ac.uk).
- N. Pinardi and M. Zavatarelli, Laboratorio di Simulazioni Numeriche del Clima e degli Ecosistemi Marini, Università degli Studi di Bologna, Piazza J. F. Kennedy 12, Palazzo Rasponi, 48100, Ravenna, Italia. (M.Zavatarelli@ambra.unibo.it; N.Pinardi@ambra.unibo.it).